Neurobiology of Disease 129 (2019) 144–158

Contents lists available at ScienceDirect

Neurobiology of Disease

journal homepage: www.elsevier.com/locate/ynbdi

RIP3 participates in early brain injury after experimental subarachnoid hemorrhage in rats by inducing necroptosis

Shuai Yuan[1], Zhengquan Yu[1], Zhuwei Zhang, Juyi Zhang, Peng Zhang, Xiang Li, Haiying Li, Haitao Shen*, Gang Chen*

Department of Neurosurgery & Brain and Nerve Research Laboratory, The First Affiliated Hospital of Soochow University, Suzhou, Jiangsu Province, China

ARTICLE INFO

Keywords:
RIP3
Subarachnoid hemorrhage
Early brain injury
Necroptosis
TNF-α
Inflammation

ABSTRACT

Necroptosis is a regulated form of necrosis that is mediated by a variety of proteins including tumor necrosis factor-α (TNF-α) and receptor-interacting proteins (RIPs). TNF-α, a critical inflammatory molecule, is one of the initiating signals in the necroptosis pathway, and RIP3 acts as a switch that commits the cell to necroptosis. Subarachnoid hemorrhage (SAH) is a common type of hemorrhagic stroke with high mortality and disability rates. RIP3 has been studied in many central nervous system (CNS) diseases, but its role in SAH has not been investigated in depth. Here, we used an autologous-blood injection model to study the role of RIP3 in brain injury induced by SAH in rats. Several indexes such as brain edema, loss of blood-brain barrier (BBB) integrity, and behavioral tests of neurological function were used to evaluate brain damage in SAH-injured rats. We found that the expression of RIP3 was increased in the rat brain after SAH, reaching the highest point 24 h post-injury. We also showed that genetic or pharmacological inhibition of RIP3 or TNF-α reduced the brain damage induced by SAH, whereas overexpression of RIP3 aggravated brain injury and neurological damage. Additionally, we verified the presence of RIP3-mediated necroptosis in an in vitro SAH model of primary cultured neurons treated with conditioned medium from primary microglia activated by oxygen hemoglobin (OxyHb). Collectively, our findings indicated that RIP3 contributed to brain damage after SAH by inducing necroptosis.

1. Introduction

Subarachnoid hemorrhage (SAH) is a common type of hemorrhagic stroke caused by blood entering the subarachnoid space (Neulen et al., 2018). This devastating cerebrovascular disease accounts for 5% of all stroke cases and has a high disability rate often leading to unforeseen death (Etminan, 2015; Yin et al., 2017). According to statistics on the etiology of SAH, intracranial aneurysms that occur in the primary bifurcations of the Circle of Willis cause about 50–85% of spontaneous SAH. Intracranial aneurysms occur in 6% of people worldwide and about 10 in 100,000 people suffer from arterial aneurysm-induced SAH every year (Schievink et al., 2004; Cahill et al., 2006). With increasing health awareness and the development of neuroimaging techniques, the detection rate of unruptured intracranial aneurysms has increased. The availability of cutting-edge neurovascular interventions allows unruptured intracranial aneurysms to be properly managed, with virtually no negative impact on the patient's quality of life or life expectancy (Dou et al., 2017). However, if an intracranial aneurysm ruptures and induces SAH, the subsequent impact is catastrophic to the patient. Therefore, effectively reducing the lethality and disability rate of SAH to improve long-term patient survival is critical importance.

The pathological mechanisms associated with SAH still remain unclear. Historically, the two primary mechanisms proposed to underlie SAH-induced brain injury were cerebral vasospasms (CVS) and early brain injury (EBI), with EBI now considered the major contributing factor (Shi et al., 2017; Leclerc et al., 2018). Neuronal necrosis and apoptosis are two critical events that occur during EBI, and some evidence has reported that inflammation also contributed to EBI after aneurysm rupture (Murakami et al., 2011; Chen et al., 2013). Accordingly, inflammatory responses have been shown to play a significant role in the progression of SAH (Lucke-Wold et al., 2016; Xie et al., 2018)

Receptor interacting proteins (RIPs) are an important branch of the serine/threonine protein kinase family. Each member of the family has its own unique functional domain in addition to a common kinase domain (Chen et al., 2017a) The diversity of the protein structure determines the special features of each member. In 1999, yeast-two-hybrid screening and bioinformatics methods were used to identify and

* Corresponding authors at: Department of Neurosurgery, The First Affiliated Hospital of Soochow University, 188 Shizi Street, Suzhou 215006, China.
E-mail addresses: m18100684632@163.com (H. Shen), sz_neurosurgery@163.com (G. Chen).
[1] These authors contributed equally to this work.

https://doi.org/10.1016/j.nbd.2019.05.004
Received 19 December 2018; Received in revised form 22 April 2019; Accepted 9 May 2019
Available online 10 May 2019
0969-9961/

analyze the proteins that bound to receptor interacting protein 1 (RIP1), which revealed a novel protein, RIP3, with high homology to RIP1 (Sun et al., 1999; Yu et al., 1999). RIP3 has two functional domains: the N-terminal serine/threonine kinase domain that is common to all members of the RIP family and a unique C-terminal domain containing a RIP-isotypic interaction motif. This C-terminal domain was found to play a key role in mediating the interaction between RIP1 and RIP3, together triggering a type of programmed necrosis called necroptosis (Meylan and Tschopp, 2005; Cho et al., 2009; Shlomovitz et al., 2017)

Apoptosis and necrosis are known to be the main types of cell death, with necrosis usually considered an unexpected and unregulated phenomenon. However, in the past thirty years, this viewpoint of necrosis has been challenged by the discovery of necroptosis and other forms of programmed necrosis that are executed via well-managed and elaborate cellular mechanisms. The discovery of necroptosis dates back to 1988 when multiple types of tumor necrosis factor (TNF)-triggered necrotic pathways were found (Laster et al., 1988). In 1998, it was reported that TNF and Fas-associated protein with death domain (FADD) induced cell death in a necrotic manner when caspase-8 was inhibited (Vercammen et al., 1998; Kawahara et al., 1998). In 2000, TNF receptors (TNFR) were shown to trigger cell death in two ways: one was caspase-8-dependent and the other depended on RIP1 in human T-cells (Holler and et a.l, 2000). In 2005, a study reported that TNFR mediated necroptosis after ischemic brain injury and necrostatin-1 could inhibit RIP1 kinase in vitro (Degterev et al., 2005). In 2009, some studies showed that RIP3 was a downstream protein of RIP1 and was essential for necroptosis (Cho et al., 2009; Zhang et al., 2009). In 2012, the mixed lineage kinase domain-like (MLKL) was identified as the executor of necroptosis in vitro (Sun et al., 2012)

Necroptosis may occur under a variety of stimulus conditions, but TNF-α is the best-studied trigger signal (Sun and Wang, 2014). TNF-α is a pleiotropic cytokine that plays a key role in inflammation caused by infection or tissue damage (Vandenabeele et al., 2010). TNF binding to TNFR1 induced the formation of complex I, which is composed of RIP1, TNFR1-associated death domain protein (TRADD), TNF receptor-associated factor 2 (TRAF2) and the cellular inhibitors of apoptosis 1/2 (cIAP1/2) (Vandenabeele et al., 2010). FADD, RIP1, and activated caspase-8 together form a death signaling complex that mediates apoptosis. When this apoptotic pathway is inhibited by cIAPs, a RIP1-RIP3 complex forms and leads to increased energy metabolism and accumulation of oxidative metabolites. These processes eventually damage the cell membrane and organelles, leasing to necroptosis. RIP1 was shown to recruit RIP3 and promote RIP3 phosphorylation via the RIP homotypic interaction motif (RHIM) (Cho et al., 2009). This triggered the formation of a cytosolic complex IIb that comprised RIP1, RIP3, FADD, and caspase-8 (Wang et al., 2008; Dondelinger et al., 2013; Feoktistova et al., 2011). If caspase-8 was inhibited or RIP3 was expressed at a high enough level, a different complex called the necrosome (including RIP1, RIP3, and MLKL) was formed (Sun et al., 2002). MLKL is considered an executor of necroptosis and was found to be phosphorylated by RIP3 at the threonine-357 and serine-358 residues (Sun et al., 2012). Phosphorylation promoted MLKL oligomerization and translocation to the plasma membrane, leading to membrane rupture and necroptotic cell death (Orozco et al., 2014; Cai et al., 2014; Chen et al., 2014; Yoon et al., 2016)

A large number of reports have indicated that necroptosis was associated with many neurological diseases such as intracerebral hemorrhage (ICH), (Shen et al., 2017) ischemic stroke, (Degterev et al., 2005) spinal cord injury (SCI), (Wang et al., 2014) traumatic brain injury (TBI), (Wang et al., 2012) and multiple sclerosis (MS) (Ofengeim et al., 2015). However, necroptosis after SAH has not been well studied. In this study, we investigated necroptosis in SAH-induced brain injury and hypothesized that RIP3 plays an important role in brain injury following SAH by mediating necroptosis.

2. Materials and methods

2.1. Experimental animals

The experimental protocols involving animals were approved by the Animal Care and Use Committee of Soochow University. All animal use, care, and operative procedures complied with the Guide for the Care and Use of Laboratory Animals by the National Institutes of Health. Adult, male, Sprague Dawley (SD) rats weighing 300–350 g were purchased from the Animal Center of Chinese Academy of Sciences, Shanghai, China. Rats were housed at a constant temperature (23 ± 1 °C) and relative humidity (40%), on a standard 12-h light/dark cycle, with free access to food and water. Sample sizes for the experiments were determined using power analyses, and every effort was made to reduce the number of animals used, as well as their pain and suffering.

2.2. In vivo SAH model in rats

As previously reported, we induced SAH by injecting autologous blood into the prechiasmatic cistern of rats (Wang et al., 2013). After an intraperitoneal injection of 4% chloral hydrate (10 ml/kg) to anesthetize the animal, the rat was positioned in a stereotaxic frame. Then, a side-port needle (with a rounded tip and an opening on the side) was stereoscopically inserted into the prechiasmatic cistern. The needle was inserted at the midline and 7.5 mm anterior to bregma, at a 45° angle to the sagittal plane, with the side-port opening of the needle facing the right side. It was lowered until the tip reached the base of the skull (2–3 mm before the chiasma) and then retracted 0.5 mm. Bone wax was used to prevent blood and cerebrospinal fluid (CSF) loss from the midline when deemed necessary. Next, 0.3 ml fresh non-heparinized autologous arterial blood was slowly injected into the prechiasmatic cistern for 20 s with a syringe pump. The rats in the Sham group were injected with 0.3 ml physiological saline. After the SAH surgical procedure was completed, rats were injected with 5 ml 0.9% physiological saline to prevent dehydration. After 45 min of recovery, all rats were returned to their home cages. Briefly, animals were deeply anesthetized at 24 h after SAH and intracardially perfused with 60 ml ice-cold PBS followed by 60 ml of 10% paraformaldehyde through the upper part of the body. The brain tissue around the bottom of the temporal lobe was collected and analyzed. Fig. S4A shows a schematic of the area used for analysis.

2.3. Neuron and microglia culture

As described previously, primary neurons from embryonic-day 18 rat embryos were isolated and cultured (Shen et al., 2017). First, the blood vessels and meninges were removed from the cerebral hemispheres. Then, the brain tissue was digested for 5 min with 0.25% trypsin (GIBCO, Carlsbad, CA, USA) and centrifuged at 1000*g* for 5 min. The pellet was resuspended in Neurobasal medium supplemented with 2% B27, 0.5 mM GlutaMAX TM-I, 50 U/ml penicillin, and 50 U/ml streptomycin (all from GIBCO, USA). Finally, neurons were plated at a density of 20,000 cells/cm^2 onto 6-well plates (Corning, NY, USA) precoated with 0.1 mg/ml poly-D-lysine (Sigma-Aldrich, St. Louis, MO, USA) and cultured in fresh Neurobasal medium. The cultures were maintained in a 5% CO_2 atmospheric incubator at 37 °C for two weeks, during which half of the culture medium was replaced every two days.

In addition, the whole brains of 1-day-old rats were used to culture primary microglia (Shen et al., 2017). The microglia were exposed to 10 μM oxygen hemoglobin (OxyHb) for 24 h, and the supernatant was collected as “Condition Medium”. The Condition Medium was centrifuged at 12,000*g* for 10 min and then filtered through a 0.22 μm syringe-filter for further experiments. This processed Conditioned Medium from the cultures of primary microglia was then used to replace half the medium of the neuronal culture for a 6-h incubation to

induce an in vitro model of SAH.

2.4. Experimental design

2.4.1. Experiment 1 Time course of the protein levels of RIP3 after SAH

For this experiment, 48 rats were randomly divided into 8 groups of 6 rats each: Sham group and 7 experimental groups of rats euthanized at specific time points after SAH (3 h, 6 h, 12 h, 24 h, 48 h, 72 h, and 7 d).

2.4.2. Experiment 2 Experimental design for studying the roles of RIP3 and its possible mechanisms in brain injury of rats after SAH

In this experiment, 240 rats were randomly divided into the following 10 groups (n = 24 per group): Sham, SAH, SAH + Vehicle, SAH + GSK872, SAH + TNF-α inhibitor (6,7-Dimethyl-3-((methyl-(2-(methyl-(1-(3-trifluoromethyl-phenyl)-1H-indol-3-ylmethyl)-amino)-ethyl)-amino)-methyl)-chromen-4-one,diHCl), SAH + GSK872 + TNF-α inhibitor, SAH + Si-NC (SiRNA-Negative Control), SAH + Si-RIP3, SAH + Vector, and SAH + Over-RIP3. At 24 h after SAH, the rats were euthanized and brain tissue from the bottom of the temporal lobe was collected.

2.4.3. Experiment 3 Experimental design for exploring the roles of RIP3 in vitro

Primary cultured neurons were divided into 4 groups: Control, Conditioned Medium, Conditioned Medium + Vehicle, and Conditioned Medium + GSK872. Detailed experimental information about each group is shown in Fig. S4B-D.

2.5. Drug administration

Drug concentrations were determined as previously described with some modifications (He et al., 2005; Tao et al., 2016). The RIP3 inhibitor GSK872 (Merck Millipore, Billerica, MA, USA) and TNF-α inhibitor (Santa Cruz Biotechnology, Santa Cruz, CA, USA) were dissolved in DMSO at concentrations of 50 mg/ml and 25 mg/ml respectively. GSK872 (3.3 mg/kg) and TNF-α inhibitor (1.65 mg/kg) were injected into the lateral cerebral ventricle of rats 24 h before SAH induction. For in vitro experiment, the GSK872 was also dissolved in DMSO at a final concentration of 1 μM in a neuronal medium.

2.6. Transfection of plasmids and small interfering RNA (siRNA) in vivo

Two types of plasmids were used in this experiment: one overexpressed rat RIP3 (Over-RIP3; Gene ID: 246240) and the other was an empty-vector plasmid (Vector) used as a negative control for Over-RIP3. Over-RIP3 and Vector were produced by Genescript (Nanjing, China). Both were stored at −80 °C and diluted to 0.5 mg/ml in enhanced transfection solution (Genescript, Nanjing, China) before intracerebroventricular injection in rats.

Two types of siRNAs from Genescript were used in this study: one was specific to rat RIP3 mRNA (Si-RIP3) to silence its transcription and the other was a scramble siRNA (Si-NC). The RIP3 siRNA sequences were as follows:

(sense) 5′-GGAAAGGCTTCTAAAGCAA dTdT- 3′ and.

(antisense) 3′- dTdTCCUUUCCGAAGAUUUCGUU-5′.

According to the manufacturer's instructions for Entranster-in vivo RNA transfection reagent (Engreen, Shanghai, China), 500 pmol RIP3 siRNA and 500 pmol scramble siRNA were dissolved in 5 μl RNase-free water. Next, 10 μl Entranster-in vivo RNA transfection reagent was added to 5 μl scramble siRNA or RIP3 siRNA solution, and the solution was mixed for 15 min. Finally, the Entranster-in vivo-siRNA mixtures were injected intracerebroventricularly into rats 24 h prior to inducing SAH.

2.7. Propidium iodide (PI) staining

The PI marker was used to test for the presence of necroptosis and the staining procedure was slightly modified from previous studies (Chen et al., 2017a) Two hours before euthanasia, PI (Sigma-Aldrich, St. Louis, MO, USA) was diluted in physiological saline and intraperitoneally injected (1 μg/g) into the rats. PI staining was observed in frozen brain sections (10 μm thick) and photographed immediately. At least one section from each rat in each group was analyzed by a researcher who was blinded to the design of the experiment.

2.8. Western blotting

Western blotting was carried out as described previously (Li et al., 2014). The brain samples were mechanically lysed with RIPA lysis buffer containing phenylmethylsulfonyl fluoride (PMSF) (both from Beyotime Institute of Biotechnology, Shanghai, China). The protein concentrations of the brain samples were determined by the bicinchoninic acid (BCA) method (enhanced BCA protein assay kit, Beyotime Institute of Biotechnology, Shanghai, China). Molecular weight marker (5 μl/lane; Thermos Scientific, Waltham, MA, USA) and protein samples (20 μg/lane) were loaded on a 10% sodium dodecyl-polyacrylamide electrophoresis (SDS-PAGE) gel, separated, and electrophoretically transferred to a polyvinylidene difluoride (PVDF) membrane (Millipore Corporation, Billerica, MA, USA). The membrane was then incubated with 5% bovine serum albumin (BSA, BIOSHARP, Hefei, China) for 1 h at room temperature to block non-specific binding. Subsequently, the membrane was incubated with one of the following primary antibodies overnight at 4 °C: anti-RIP1, -RIP3, -MLKL, -caspase-8, -p-Ser (all from Santa Cruz Biotechnology, Santa Cruz, CA, USA), or anti-albumin (Abcam, Cambridge, UK). The β-tubulin antibody was diluted at 1:5000 and used as the loading control. Next, the membrane was incubated with species-specific horseradish peroxidase (HRP)-conjugated secondary antibodies (Santa Cruz Biotechnology, Santa Cruz, CA, USA) for 2 h at room temperature and washed with phosphate-buffered saline containing 0.1% Tween-20 (PBST). The protein signal was detected using an enhanced chemiluminescence (ECL) kit (Beyotime, Shanghai, China). The relative density of protein was analyzed using ImageJ software (NIH, Bethesda, MD, USA) and normalized to that of the corresponding loading control. Phosphorylation levels were determined by calculating the ratio of the phospho-protein to total protein.

2.9. Immunofluorescence

Immunofluorescent staining was performed on coronal brain sections containing the basal temporal lobe (Dou et al., 2017). Sections were incubated with primary antibodies specific to RIP1, RIP3, and MLKL overnight at 4 °C. They were then washed three times with PBST and incubated with the corresponding secondary antibodies at 37 °C for 1 h. Next, sections were treated with 4,6-diamino-2-phenylindole (DAPI, SouthernBiotech, Birmingham, USA) and coverslipped. Finally, fluorescence in these brain sections were visualized under a fluorescence microscope and analyzed for relative fluorescence intensity using Image J software. At least one slice from each rat was stained, and at least three photomicrographs were captured per slice. In the quantitative analysis, at least one photomicrograph from each rat in various groups was included.

2.10. Immunoprecipitation

Immunoprecipitation was performed as described previously (Shen et al., 2017). First, the brain samples were lysed in RIPA lysis buffer. Then, the lysate was incubated while orbital shaking overnight at 4 °C with a specific antibody or rabbit IgG (negative control). Then, protein A + G Sepharose beads (Santa Cruz Biotechnology, Santa Cruz, CA, USA) were added to each immune complex, and the lysate mixture was

incubated with orbital shaking for 4 h at 4 °C. SDS-PAGE and immunoblotting were then performed for protein separation and detection.

2.11. Blood-brain barrier (BBB) injury

BBB permeability was evaluated by albumin extravasation (Li et al., 2016). Under normal circumstances, the concentration of albumin in brain is very low due to the presence of the BBB. However, after the BBB is damaged, the albumin content in the central nervous system (CNS) increases significantly. Therefore, changes in albumin concentration in brain tissue can be used as an indicator to assess the extent of BBB damage. We used western blotting to detect the protein levels of albumin in rat brain tissue from various groups.

Additionally, as described in a previous report, (Wu et al., 2017a) to quantify low-molecularweight molecular leakage, we injected with 2% FITC-dextran (100 μg/ml, 0.2 ml; Sigma-Aldrich, St. Louis, MO, USA) to rats. Two hours later, the rats were subjected to systemic intracardiac perfusion with 1 USP U/ml heparin in saline to flush the FITC-dextran out of the vasculature. 5 min later, the rats were euthanized, and their perfused brains were subsequently harvested. Supernatant fluorescence was measured using an EnSpire Manager Multimode Plate Reader (PerkinElmer, Waltham, MA, USA).

2.12. Brain edema

The brain-edema index was assessed using a wet/dry method as previously described (Suzuki et al., 2010). Briefly, brain tissue was collected and immediately weighed (recorded as the wet weight). Then the tissue was dried at 100 °C for 72 h and weighed again to obtain the dry weight. The percentage of brain water content was calculated as [(wet weight − dry weight)/wet weight] × 100%.

2.13. Enzyme-linked immunosorbent assay (ELISA) of TNF-α

The concentration of TNF-α in the cerebrospinal fluid (CSF) of rats was determined by ELISA. This assay was performed according to the manufacturer's instructions (Bio-Swamp, Hubei, China).

2.14. Behavioral tests for neurological impairment

At 24 h after SAH, 12 rats in each group in Experiment 2 were selected randomly and then tested for behavioral defects using a battery of behavioral tasks and a previously published scoring system (Cao et al., 2018). The behavioral and activity scores of each rat were assessed by an individual who was blinded to the experimental groups (details are shown in Table 1).

2.15. Morris water maze

The Morris water maze (MWM) was performed as described previously (Wu et al., 2017b) The MWM consisted of a circular pool of 2 m in diameter and 0.75 m in height. It was filled with water to a depth of 0.4 m and maintained at room temperature. Melanin was added to the water. Four equidistant points were arbitrarily designated as North (N), South (S), East (E), and West (W), which established four quadrants (NW, NE, SE, and SW). The area of the pool within 20 cm of the outer wall was designated as the perimeter for the assessment of thigmotaxis. The annulus was defined as a 30-cm diameter circle surrounding the platform. A transparent plexiglass platform (10 cm × 10 cm) was located at the convergence point of eight equidistant random lines (N, S, E, W, NW, NE, SE, and SW), submerged 2 cm below the water surface. A camera mounted on the ceiling above the pool tracked the movement of the rats. The MWM behavioral test was conducted during the light cycle between 10:00 and 18:00.

Table 1
Neurobehavioral evaluation.

Category	Behavior	Score
Appetite	Finished meal	0
	Left meal unfinished	1
	Scarcely ate	2
Activity	Walk and reach at least three corners of the cage	0
	Walk with some stimulations	1
	Almost always lying down	2
Deficits	No deficits	0
	Unstable walk	1
	Impossible to walk	2

2.16. Statistical analysis

All data are expressed as the mean ± standard error of the mean (SEM). We tested the normality of the data sets with the Kolmogorov-Smirnov test. Data groups (two groups) with normal distributions were compared using the two-tailed unpaired Student's *t*-test, and the Mann Whitney *U* test was used for nonparametric data. $P < 0.05$ was considered statistically significant.

3. Results

3.1. General observations

After the Sham or SAH surgery, the heart rate, blood pressure, and body temperature of the rats were monitored in real-time. No significant changes in heart rate, mean arterial blood pressure, or body temperature were detected in any of the SAH experimental groups (data not shown).

3.2. The level of RIP3 was greatly increased in the rat brain after SAH

To detect the dynamic changes in the expression of RIP3 after SAH, western blotting and immunofluorescent staining were performed. The results of the western blotting revealed that, compared with Sham group, the expression of RIP3 increased after SAH, reaching the highest point at 24 h and then recovering gradually ($P < 0.05$, Fig. 1A and B). Immunofluorescent staining also showed that the expression of RIP3 was significantly increased at 24 h after SAH ($P < 0.05$, Fig. 2C). Therefore, 24 h was considered an appropriate time point for further study.

3.3. Necroptosis was detected in the brain tissue of rats after SAH

We used frozen brain sections to perform PI staining and observed the number of PI-positive cells in Sham group compared with 24 h post-SAH groups. The results indicated that the number of PI-positive cells in the brain tissue of Sham rats was very low. In contrast, the number of PI-positive cells reached very high levels in the brain tissue at 24 h after SAH induction ($P < 0.05$, Fig. 1C and D). Since the necrosome (a complex composed of RIP3, RIP1, and MLKL) is known to play an important role in necroptosis, we immunoprecipitated RIP3 and then immunoblotted with antibodies against RIP1 and MLKL. We found that interactions between RIP3 and RIP1, as well as RIP3 and MLKL, were significantly increased after SAH compared with Sham group (both $P < 0.05$, Fig. 2A and B). As shown in Fig. 2D and E, immunofluorescence staining for RIP1, RIP3, and MLKL at 24 h after SAH revealed that SAH induced a clear increase in these protein levels (all $P < 0.05$). Taken together, these results indicated the presence of the necrosome in the rat brain after SAH.

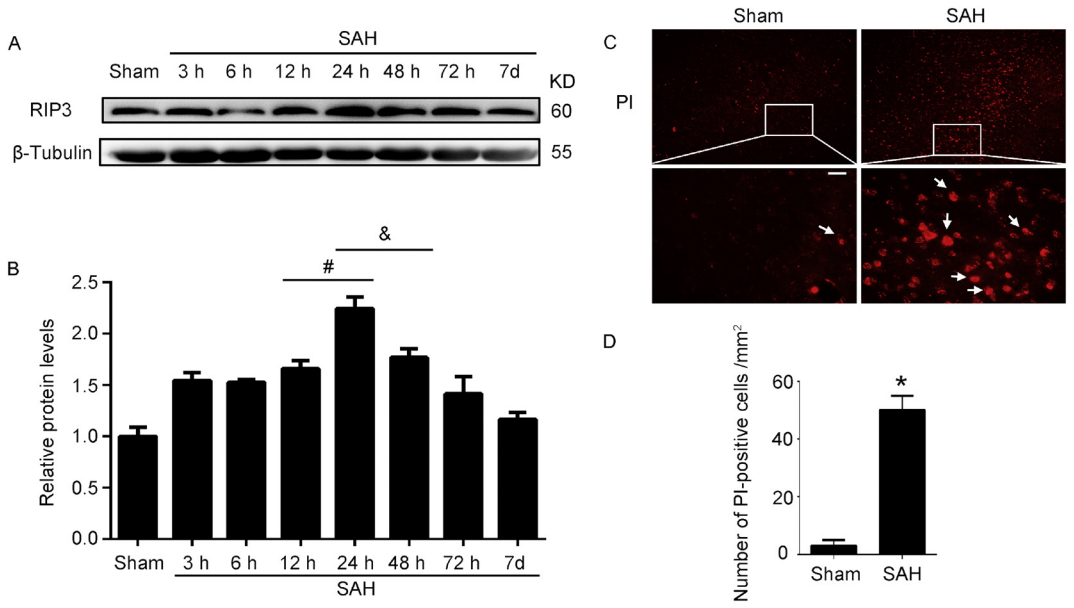

Fig. 1. The expression of RIP3 and number of PI-positive cells were increased after SAH. (A) Western blotting showed the protein levels of RIP3 at 3, 6, 12, 24, 48, 72 h, and 7 d after SAH. (B) Quantification of RIP3. Protein levels were normalized to that of β-tubulin; $^{*}P < 0.05$ vs. Sham group, $^{\#}P < 0.05$ vs. SAH (24 h) group, $^{\&}P < 0.05$ vs. SAH (24 h) group, n = 6. (C) Representative photographs of PI staining in the Sham group and SAH 24 h group. Scale bar = 100 μm. Arrows point to PI-positive cells. (D) PI-positive cells/mm^2 was quantified,$^{*}P < 0.05$ vs. Sham group. Data were expressed as means ± SEM, n = 6.

3.4. Pharmacological interventions attenuated the increased phosphorylation of RIP3 and MLKL and inhibited brain damage induced by SAH

In order to test the role of RIP3 in brain injury after SAH, we used GSK872, a pharmacological inhibitor of RIP3. We also used a TNF-α inhibitor to determine the relationship between RIP3 and the TNF-α signaling pathway. We performed PI staining to observe the number of PI-positive cells in the SAH + GSK872, SAH + TNF-α inhibitor, and SAH + GSK872 + TNF-α inhibitor groups. As shown in Fig. 3A, treatment with GSK872, TNF-α inhibitor, and GSK872 + TNF-α inhibitor significantly decreased the number of PI-positive cells compared with the SAH + Vehicle group (all $P < 0.05$, Fig. 3B). However, there were no statistical differences between SAH + GSK872 + TNF-α inhibitor group and SAH + GSK872 or SAH + TNF-α inhibitor groups (both $P > 0.05$, Fig. 3B).

We also used immunoprecipitation to analyze the phosphorylation of RIP3 and MLKL in the brain tissue after treatment with GSK872, TNF-α inhibitor, or GSK872&TNF-α inhibitor. The results showed that the phosphorylation of RIP3 in the SAH group was significantly higher than Sham group ($P < 0.05$, Fig. 3C-E). In contrast, the phosphorylation of RIP3 in the SAH + SK872 and SAH + TNF-α inhibitor groups was decreased compared with the SAH + Vehicle group respectively (both $P < 0.05$, Fig. 3C–E). We observed similar results for MLKL phosphorylation; the phosphorylation of MLKL in SAH group was significantly increased compared with Sham group ($P < 0.05$, Fig. 3F–H), and the phosphorylation levels of MLKL in the SAH + GSK872 and SAH + TNF-α inhibitor groups were decreased compared with the SAH + Vehicle group respectively (both $P < 0.05$, Fig. 3F–H).

Next, we examined SAH-induced damage to the BBB by measuring albumin extravasation. The protein level of albumin in SAH group was significantly higher than that of Sham group. The albumin levels in SAH + GSK872, SAH + TNF-α inhibitor, and SAH + GSK872 + TNF-α inhibitor groups were significantly decreased compared with SAH + Vehicle group (all $P < 0.05$, Fig. 4A and B). However, there were no statistical differences between SAH + GSK872 + TNF-α inhibitor group and SAH + GSK872 or SAH + TNF-α inhibitor groups (both $P > 0.05$, Fig. 4A and B). In addition, FITC-dextran is commonly used to measure BBB permeability; it was used in the present study. These results indicated that there was a higher level of FITC-dextran fluorescence in SAH group compared with Sham group; RIP3 inhibition and TNF-α inhibitor treatment in SAH rats could reduce BBB injury (all $P < 0.05$, Fig. 4C).

Finally, we evaluated the level of brain edema induced by SAH in various groups. The SAH group showed more severe brain edema than Sham group. However, brain edema decreased significantly following the interventions of GSK872 and TNF-α inhibitor (all $P < 0.05$, Fig. 4D). We also found no statistical differences in brain edema between the SAH + GSK872 + TNF-α inhibitor group and the SAH + GSK872 or SAH + TNF-α inhibitor groups (both $P > 0.05$, Fig. 4D).

3.5. Effects of genetic knockdown of RIP3 on brain injury following SAH

We used PI staining to detect the number of PI-positive cells in SAH-injured rats transfected with Si-RIP3 to knock down RIP3 or SAH-injured rats transfected with the Over-RIP3 plasmid to overexpress RIP3. We found that the number of PI-positive cells in SAH + Si-RIP3 group was significantly decreased compared with SAH + Si-NC group ($P < 0.05$, Fig. 5A and B), and the number of PI-positive cells in the SAH + Over-RIP3 group was increased compared with the corresponding control SAH + Vector group ($P < 0.05$, Fig. 5A and B). There were no statistical differences between SAH group and SAH + Si-NC or SAH + Vector groups (both $P > 0.05$, Fig. 5A and B).

We also immunoprecipitated RIP3 and examined its level of phosphorylation. The phosphorylation of RIP3 in SAH group was significantly increased compared with Sham group. RIP3 phosphorylation in the SAH + Si-RIP3 group was decreased compared with SAH + Si-NC group, and the phosphorylation of RIP3 in the SAH + Over-RIP3 group was increased compared with SAH + Vector group (all $P < 0.05$, Fig. 5C–E). Similarly, we tested the phosphorylation of MLKL immunoprecipitated from rat brain tissue after SAH and found that the phosphorylation of MLKL in SAH group was significantly increased compared with Sham group. Similar to the results observed for RIP3 phosphorylation, the phosphorylation of MLKL in SAH + Si-RIP3 group was decreased compared with SAH + Si-NC group, and the phosphorylation of MLKL in SAH + Over-RIP3 group was increased compared with SAH + Vector group (all $P < 0.05$, Fig. 5F–H).

Finally, we assessed SAH-induced brain damage in Si-RIP3- and

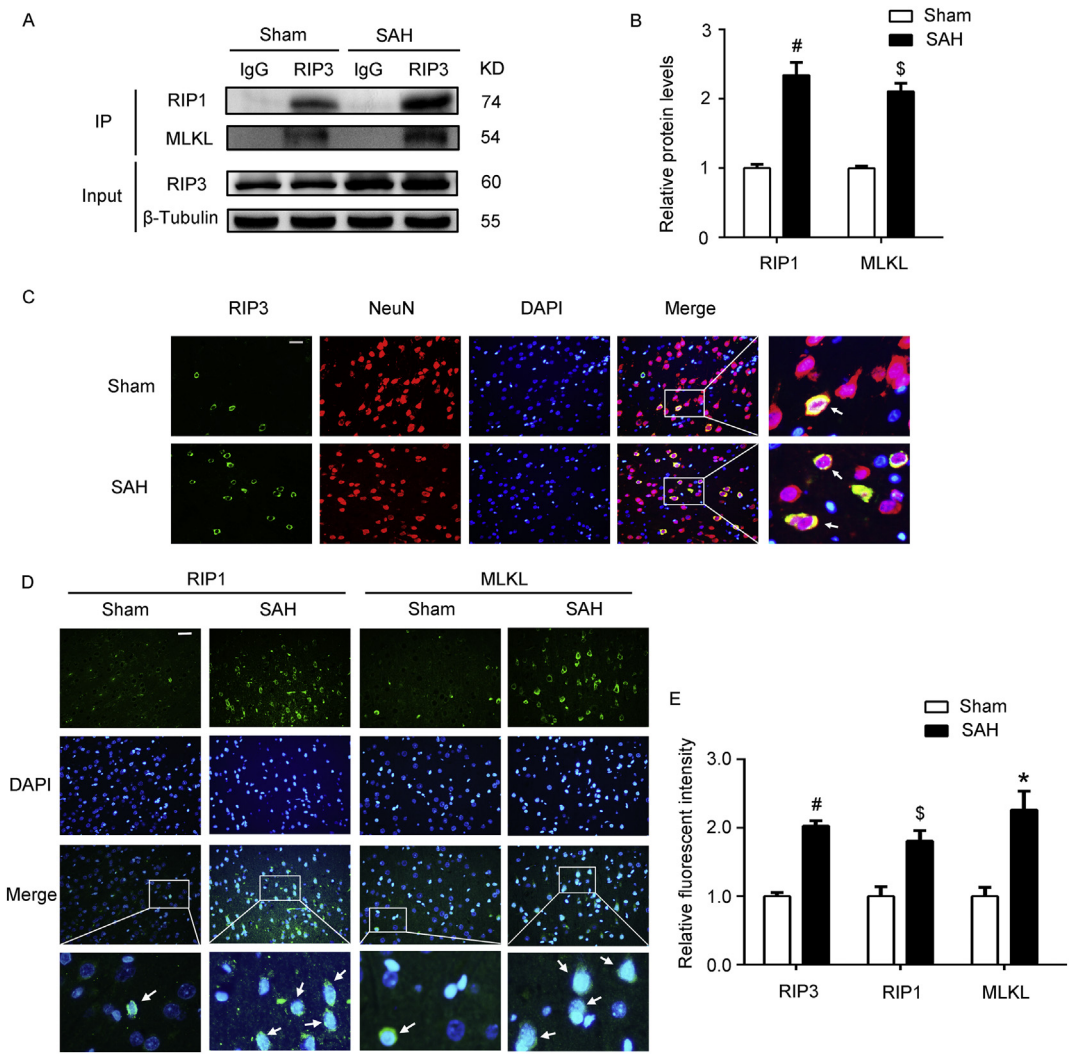

Fig. 2. The formation of necrosome. (A) Immunoprecipitation (IP) of cell lysates with RIP3 antibody. (B) Quantitative analysis of IP; $^{\#}P < 0.05$, and $^{\$}P < .05$ vs. Sham group. (C) Double immunofluorescence analysis was performed with antibody for RIP3 (green) and neuron marker (NeuN, red) in brain sections. Nuclei were labeled with DAPI (blue). Representative images of Sham group and SAH (24 h) group were shown. The squares in merged images were magnified as representative pictures, and arrows pointed to RIP3 + NeuN + cells. Scale bar = 100 μm. (D) Immunofluorescence analysis was respectively performed with antibodies against RIP3, RIP1, MLKL (green) and nuclei were labeled with DAPI (blue). Representative images of Sham group and SAH (24 h) group were shown. The squares in merged images were magnified as representative pictures, and arrows pointed to RIP1 + and MLKL + cells. Scale bar = 100 μm. (E) The relative fluorescent intensity of RIP3, RIP1, and MLKL were shown; $^{\#}P < 0.05$, $^{\$}P < 0.05$, and $^{*}P < 0.05$ vs. Sham group. Data were means ± SEM, n = 6. (For interpretation of the references to colour in this figure legend, the reader is referred to the web version of this article.)

Over-RIP3-transfected rats by examining the integrity of the BBB and the level of brain edema. We found that the protein levels of albumin in the brain tissue of rats in SAH and SAH + Over-RIP3 groups were higher than those in Sham and SAH + Vector groups, respectively, whereas the albumin levels observed in SAH + Si-RIP3 group were lower than that in SAH + Si-NC group (all $P < 0.05$, Fig. 6A and B). Additionally, the results of FITC-dextran level analysis indicated that RIP3 knockdown in SAH rats could reduce BBB injury, while over-expression of RIP3 showed opposite results (both $P < 0.05$, Fig. 6C). The SAH group showed more serious brain edema than Sham group, as did the SAH + Over-RIP3 group compared with SAH + Vector group. On the contrary, Si-RIP3 relieved the brain edema induced by SAH (all $P < 0.05$, Fig. 6D).

3.6. The level of TNF-α in the CSF was decreased after inhibition of RIP3 and increased after upregulation of RIP3

The concentration of TNF-α in the CSF of rats was detected by ELISA in the different experimental and their corresponding control groups. Compared with Sham group, the concentration of TNF-α was significantly increased in SAH group. Compared with SAH group, neither the Vehicle treatment nor transfection with Si-NC or the empty-vector plasmid had any obvious effects on the levels of TNF-α in the CSF (all $P > 0.05$, Figs. 4E and 6E). However, treatment with GSK872, TNF-α inhibitor, or transfection with Si-RIP3 significantly reduced the levels of TNF-α compared with their corresponding control groups, while upregulation of RIP3 by transfection with Over-RIP3 elevated the levels of TNF-α in rat CSF (all $P < 0.05$, Figs. 4E and 6E).

3.7. Pharmacological or genetic inhibition of RIP3 improved neurocognitive function of rats following SAH

We assessed the neurocognitive function of rats following SAH by conducting a battery of behavioral tests (that generate neurological scores), as well as the MWM test to investigate spatial and motor learning. Compared with Sham group, the neurological scores of SAH group were significantly increased, indicating that rats with SAH exhibited clear neurological deficits. Vehicle treatment had no significant

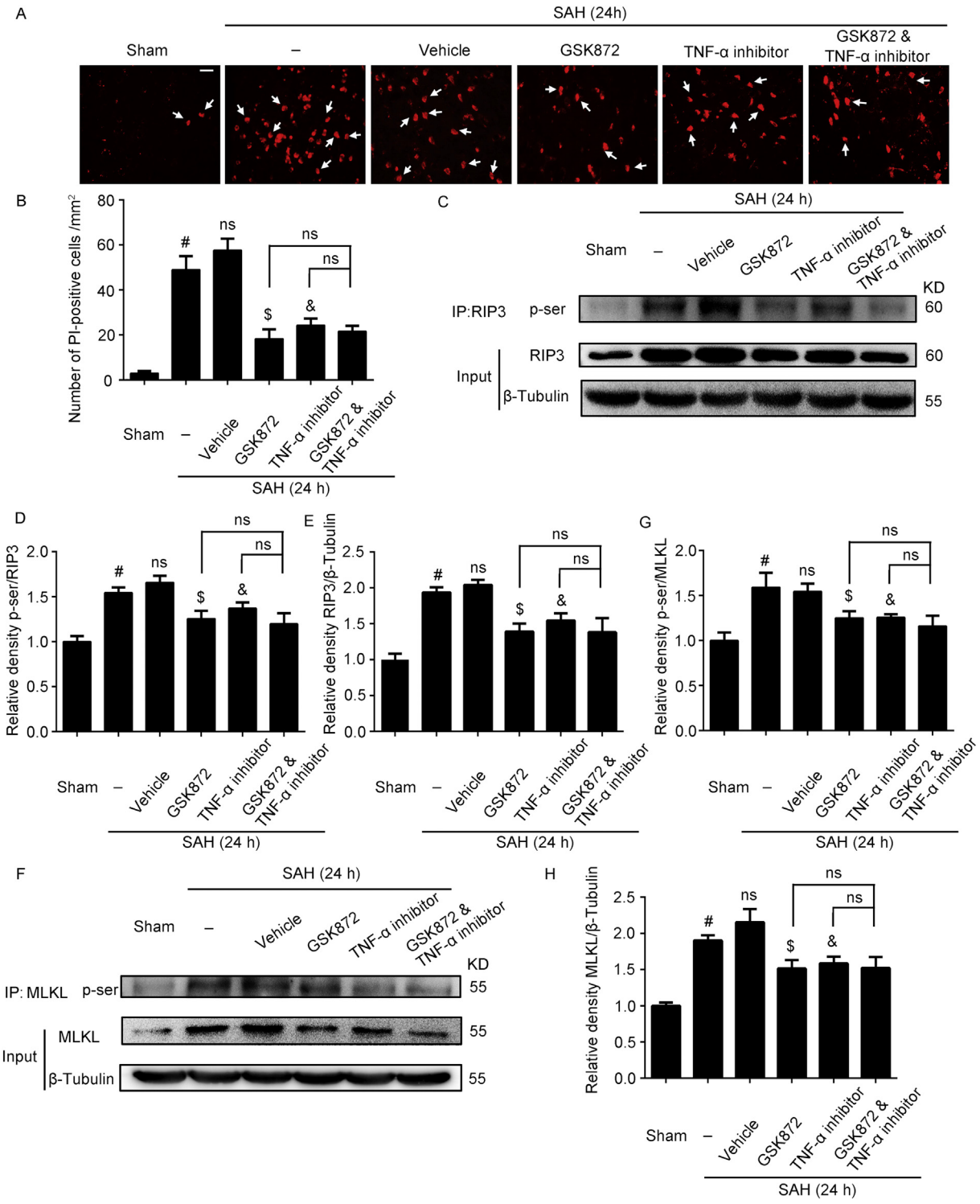

Fig. 3. Effects of GSK872 and/or TNF-α inhibitor on the phosphorylation of RIP3 and MLKL. (A) Representative photographs of PI staining in Sham, SAH, SAH + Vehicle, SAH + GSK872, SAH + TNF-α inhibitor, and SAH + GSK872&TNF-α inhibitor groups. Scale bar = 100 μm. Arrows point to PI-positive cells. (B) PI-positive cells/mm^2 was quantified; $^{\#}P < 0.05$ vs. Sham group; ns, no significant difference vs. SAH group; $^{\$}P < 0.05$ vs. SAH + Vehicle group; $^{\&}P < 0.05$ vs. SAH + Vehicle group; ns, no significant difference vs. SAH + GSK872 group; ns, no significant difference vs. SAH + TNF-α inhibitor group. (C) Immunoprecipitation (IP) of cell lysates with RIP3 antibody. (D) Quantitative analysis of IP (p-ser/RIP3); $^{\#}P < 0.05$ vs. Sham group; ns, no significant difference vs. SAH group; $^{\$}P < 0.05$ vs. SAH + Vehicle group; $^{\&}P < 0.05$ vs. SAH + Vehicle group; ns, no significant difference vs. SAH + GSK872 group; ns, no significant difference vs. SAH + TNF-α inhibitor group. (E) Quantitative analysis of IP (RIP3/β-tubulin); $^{\#}P < 0.05$ vs. Sham group; ns, no significant difference vs. SAH group; $^{\$}P < 0.05$ vs. SAH + Vehicle group; $^{\&}P < 0.05$ vs. SAH + Vehicle group; ns, no significant difference vs. SAH + GSK872 group; ns, no significant difference vs. SAH + TNF-α inhibitor group. (F) IP of cell lysates with MLKL antibody. (G) Quantitative analysis of IP (p-ser/MLKL); $^{\#}P < 0.05$ vs. Sham group; ns, no significant difference vs. SAH group; $^{\$}P < 0.05$ vs. SAH + Vehicle group; $^{\&}P < 0.05$ vs. SAH + Vehicle group; ns, no significant difference vs. SAH + GSK872 group; ns, no significant difference vs. SAH + TNF-α inhibitor group. (H) Quantitative analysis of IP (MLKL/β-tubulin); $^{\#}P < 0.05$ vs. Sham group; ns, no significant difference vs. SAH group; $^{\$}P < 0.05$ vs. SAH + Vehicle group; $^{\&}P < 0.05$ vs. SAH + Vehicle group; ns, no significant difference vs. SAH + GSK872 group; ns, no significant difference vs. SAH + TNF-α inhibitor group. All data were means ± SEM, n = 6.

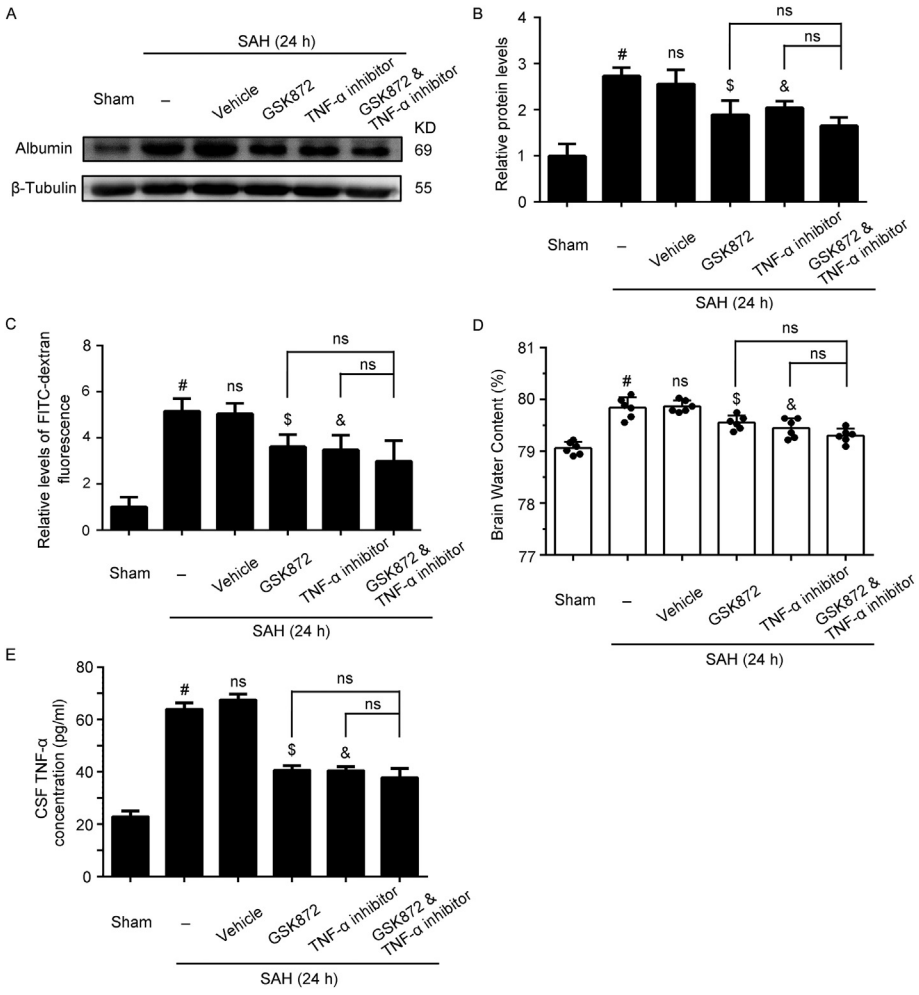

Fig. 4. Evaluation of BBB damage by albumin extravasation and brain edema assessment by brain water content after treatment with inhibitors. (A) Western blotting of albumin levels after the intervention of GSK872, TNF-α inhibitor and GSK872& TNF-α inhibitor. (B) Quantitative analysis of the levels of albumin. Protein levels were normalized to that of β-tubulin; mean values of quantification of Sham group were normalized to 1.0; $^{\#}P < 0.05$ vs. Sham group; ns, no significant difference vs. SAH group; $^{\$}P < 0.05$ vs. SAH + Vehicle group; $^{\&}P < 0.05$ vs. SAH + Vehicle group; ns, no significant difference vs. SAH + GSK872 group; ns, no significant difference vs. SAH + TNF-α inhibitor group. (C) The relative level of FITC-dextran fluorescence in each group. Mean values of quantification of Sham group were normalized to 1.0; $^{\#}P < 0.05$ vs. Sham group; ns, no significant difference vs. SAH group; $^{\$}P < 0.05$ vs. SAH + Vehicle group; $^{\&}P < 0.05$ vs. SAH + Vehicle group; ns, no significant difference vs. SAH + GSK872 group; ns, no significant difference vs. SAH + TNF-α inhibitor group. (D) Brain water content was performed at 24 h after SAH. Bar graphs showed the effects of GSK872 and/or TNF-α inhibitor on brain water content; $^{\#}P < 0.05$ vs. Sham group; ns, no significant difference vs. SAH group; $^{\$}P < 0.05$ vs. SAH + Vehicle group; $^{\&}P < 0.05$ vs. SAH + Vehicle group; ns, no significant difference vs. SAH + GSK872 group; ns, no significant difference vs. SAH + TNF-α inhibitor group. (E) The concentration of TNF-α was determined by ELISA; $^{\#}P < 0.05$ vs. Sham group; ns, no significant difference vs. SAH group; $^{\$}P < 0.05$ vs. SAH + Vehicle group; $^{\&}P < 0.05$ vs. SAH + Vehicle group; ns, no significant difference vs. SAH + GSK872 group; ns, no significant difference vs. SAH + TNF-α inhibitor group. Data were mean ± SEM, n = 6.

effect on cognitive function in SAH rats, but GSK872 or TNF-α inhibitor administration was able to relieve the neurological deficits compared with those of SAH + Vehicle group. Meanwhile, Si-RIP3 improved the neurological scores in SAH injured rats compared with the rats in SAH + Si-NC group and Over-RIP3 aggravated the neurological deficits compared with SAH + Vector group. We found no statistically significant differences between SAH group and SAH + Si-NC or SAH + Vector groups (details showed in Table 2).

In the MWM test, the escape latencies of rats in SAH group were significantly increased compared with those in Sham group. The escape latencies of the SAH + GSK872, SAH + TNF-α inhibitor, and SAH + GSK872 + TNF-α inhibitor groups were decreased compared with SAH + Vehicle group. The swim distance of the SAH group was also significantly increased compared with Sham group, and the swim distances of the SAH + GSK872, SAH + TNF-α inhibitor, and SAH + GSK872 + TNF-α inhibitor groups were decreased compared with SAH + Vehicle group. However, there were no statistical differences between SAH group and SAH + Vehicle group. We found that the escape latency of the SAH + Si-RIP3 group was significantly decreased compared with SAH + Si-NC group, whereas the escape latency of SAH + Over-RIP3 group was significantly increased compared with SAH + Vector group. Similarly, the swim distance of the SAH + Si-RIP3 group was decreased compared with SAH + Si-NC group, and the swim distance of SAH + Over-RIP3 group was increased compared with SAH + Vector group (Fig. 7).

3.8. GSK872 inhibited the phosphorylation of RIP3 and MLKL in vitro

In order to further verify the role of RIP3 in brain injury, we performed experiments in an in vitro model of SAH (neuronal culture exposed to Condition Medium). Neurons exposed to the Condition Medium were then immunoprecipitated for RIP3. Immunoblotting of the immunoprecipitated RIP3 samples indicated that after Condition Medium stimulation, interactions between RIP3 and RIP1, as well as RIP3 and MLKL, were significantly increased in neurons compared with Control group (both $P < 0.05$, Fig. 8A and B). We also immunoprecipitated RIP3 to analyze its expression and phosphorylative level following Condition Medium exposure and additional GSK872 treatment. We found that the phosphorylation of RIP3 in the Condition Medium group was significantly increased compared with Control group. RIP3 phosphorylation in Conditioned Medium + GSK872 group was decreased compared with Condition Medium + Vehicle group (both $P < 0.05$, Fig. 8C–E). We additionally analyzed the phosphorylation of MLKL using the same techniques. The results showed that the phosphorylation of MLKL in Condition Medium group was significantly higher than Control group, whereas the phosphorylation of MLKL in Conditioned Medium + GSK872 group was lower than Conditioned Medium + Vehicle group (both $P < 0.05$, Fig. 8F–H).

4. Discussion

Our study supported the hypothesis that RIP3 plays an important role in brain injury induced by SAH in rats by mediating necroptosis. We revealed that the expression of RIP3 was increased in brain tissue

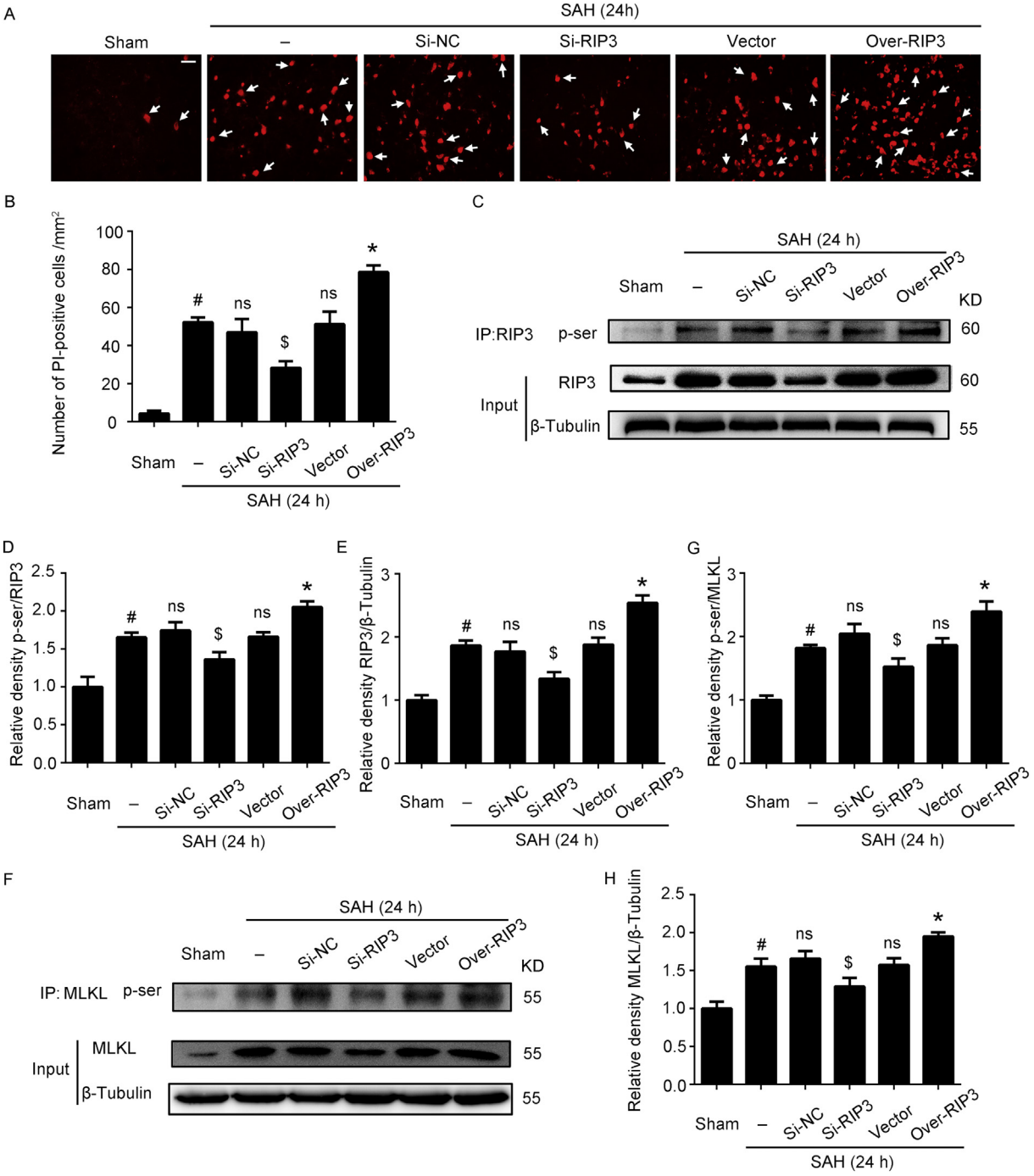

Fig. 5. Effects of Si-RIP3 and Over-RIP3 on the phosphorylation of RIP3 and MLKL. (A) Representative photographs of PI staining in various groups. Scale bar = 100 μm. Arrows point to PI-positive cells. (B) PI-positive cells/mm^2 was quantified; $^{\#}P < 0.05$ vs. Sham group; ns, no significant difference vs. SAH group; $^{\$}P < 0.05$ vs. SAH + Si-NC group; ns, no significant difference vs. SAH group; $^{*}P < 0.05$ vs. SAH + Vector group. (C) Immunoprecipitation (IP) of cell lysates with RIP3 antibody. (D) Quantitative analysis of IP (p-ser/RIP3); $^{\#}P < 0.05$ vs. Sham group; ns, no significant difference vs. SAH group; $^{\$}P < 0.05$ vs. SAH + Si-NC group; ns, no significant difference vs. SAH group; $^{*}P < 0.05$ vs. SAH + Vector group. (E) Quantitative analysis of IP (RIP3/β-tubulin); $^{\#}P < 0.05$ vs. Sham group; ns, no significant difference vs. SAH group; $^{\$}P < 0.05$ vs. SAH + Si-NC group; ns, no significant difference vs. SAH group; $^{*}P < 0.05$ vs. SAH + Vector group. (F) Immunoprecipitation (IP) of cell lysates with MLKL antibody. (G) Quantitative analysis of IP (p-ser/MLKL); $^{\#}P < 0.05$ vs. Sham group; ns, no significant difference vs. SAH group; $^{\$}P < 0.05$ vs. SAH + Si-NC group; ns, no significant difference vs. SAH group; $^{*}P < 0.05$ vs. SAH + Vector group. (H) Quantitative analysis of IP (MLKL/β-tubulin); $^{\#}P < 0.05$ vs. Sham group; ns, no significant difference vs. SAH group; $^{\$}P < 0.05$ vs. SAH + Si-NC group; ns, no significant difference vs. SAH group; $^{*}P < 0.05$ vs. SAH + Vector group. Data were mean ± SEM, n = 6.

after SAH, peaking at 24 h post-injury. PI staining was carried out to prove that there was a significant increase in necroptosis after SAH. We also showed that RIP3, RIP1, and MLKL did indeed form the necrosome complex in brain tissue after SAH. Taken together, we inferred that necroptosis imparted deleterious effects on the brain after SAH. Furthermore, we used GSK872 (a pharmacological inhibitor of RIP3), TNF-α inhibitor, Si-RIP3, and Over-RIP3 to interfere with RIP3 levels in rats prior to inducing SAH. From the results of the PI staining, we showed the pretreatments with GSK872, TNF-α inhibitor, or Si-RIP3 transfection reduced the number of PI-positive cells in brain tissue

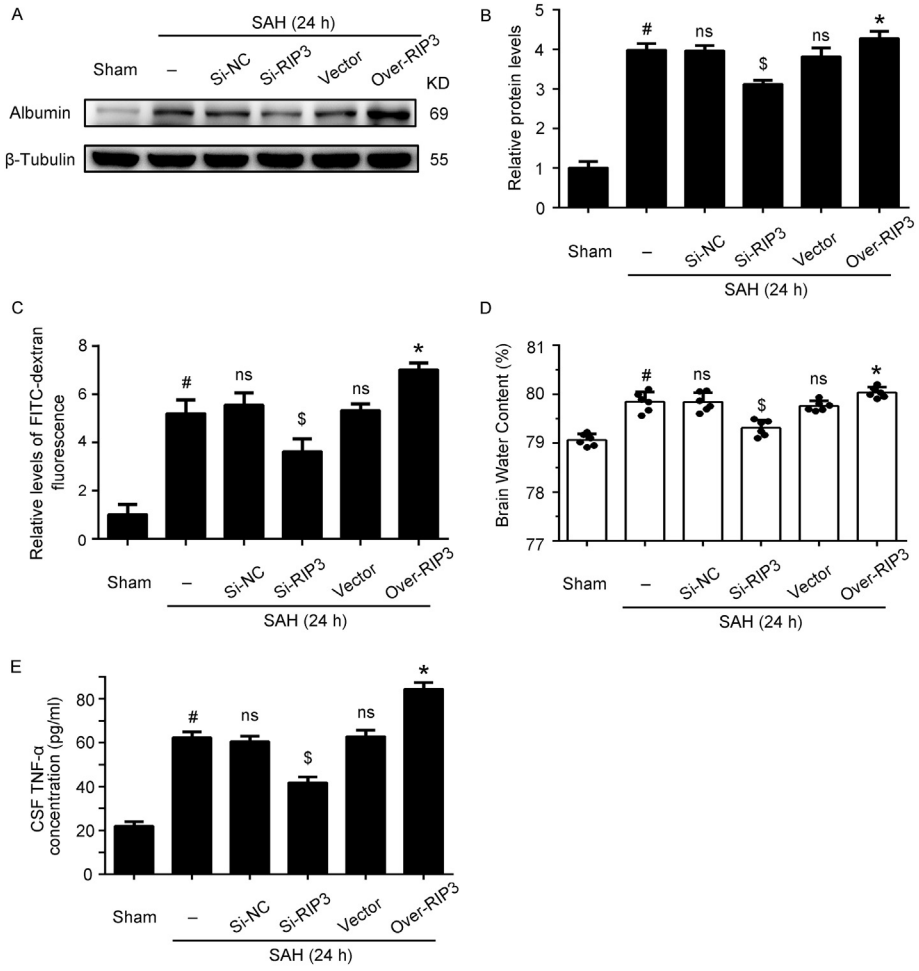

Fig. 6. Evaluation of BBB damage by albumin extravasation and brain edema assessment by brain water content in siRNA and plasmid-transfected SAH rats. (A) Western blotting showed the levels of albumin in Sham group, SAH group, SAH + Si-NC group, SAH + Si-RIP3 group, SAH + Vector group, and SAH + Over-RIP3 group. (B) Quantitative analysis of levels of albumin. Protein levels were normalized to that of β-tubulin. Mean values of quantification of Sham group were normalized to 1.0; $^{\#}P < 0.05$ vs. Sham group; ns, no significant difference vs. SAH group; $^{\$}P < 0.05$ vs. SAH + Si-NC group; ns, no significant difference vs. SAH group; $^{*}P < 0.05$ vs. SAH + Vector group. (C) The relative level of FITC-dextran fluorescence in each group. Mean values of quantification of Sham group were normalized to 1.0; $^{\#}P < 0.05$ vs. Sham group; ns, no significant difference vs. SAH group; $^{\$}P < 0.05$ vs. SAH + Si-NC group; ns, no significant difference vs. SAH group; $^{*}P < 0.05$ vs. SAH + Vector group. (D) Brain water content was measured 24 h after SAH. Bar graphs revealed the effects of Si-RIP3 and Over-RIP3 on brain water content; $^{\#}P < 0.05$ vs. Sham group; ns, no significant difference vs. SAH group; $^{\$}P < 0.05$ vs. SAH + Si-NC group; ns, no significant difference vs. SAH group; $^{*}P < 0.05$ vs. SAH + Vector group. (E) The concentrations of TNF-α were determined by ELISA; $^{\#}P < 0.05$ vs. Sham group; ns, no significant difference vs. SAH group; $^{\$}P < 0.05$ vs. SAH + Si-NC group; ns, no significant difference vs. SAH group; $^{*}P < 0.05$ vs. SAH + Vector group. Data were mean ± SEM, n = 6.

Table 2
Clinical behavior scores in each group (n = 12).

Group	Mean score
Sham	0.56
SAH	2.62[a]
SAH + Vehicle	2.68[b]
SAH + GSK872	1.56[c]
SAH + TNF-α inhibitor	1.87[d]
SAH + GSK872 & TNF-α inhibitor	1.37[e,f]
SAH + Si-NC	2.56[g]
SAH + Si-RIP3	2.06[h]
SAH + Vector	2.62[i]
SAH + Over-RIP3	3.18[j]

[a] $P < 0.05$ vs. sham group.
[b] $P > 0.05$ vs. SAH group.
[c] $P < 0.05$ vs. SAH + Vehicle group.
[d] $P < 0.05$ vs. SAH + Vehicle group.
[e] $P > 0.05$ vs. SAH + GSK872 group.
[f] $P > 0.05$ vs. SAH + TNF-α inhibitor group.
[g] $P > 0.05$ vs. SAH group.
[h] $P < 0.05$ vs. SAH + Si-NC group.
[i] $P > 0.05$ vs. SAH group.
[j] $P < 0.05$ vs. SAH + Vector group.

compared with their corresponding control groups. Meanwhile, the transfection with Over-RIP3 increased the number of PI-positive cells.

The phosphorylation of RIP3 and MLKL has also been found to be very important in the formation of the necrosome (Zhang et al., 2016; Moriwaki and Chan, 2013). We analyzed the phosphorylation of immunoprecipitated RIP3 and MLKL and found that GSK872, TNF-α inhibitor, and Si-RIP3 reduced the phosphorylation of both proteins, while Over-RIP3 increased their phosphorylation. GSK872, TNF-α inhibitor, and Si-RIP3 treatment also reduced BBB disruption and brain edema, whereas Over-RIP3 increased the destruction of the BBB and aggravated cerebral edema. Finally, in order to further verify the mechanism of necroptosis involved in brain injury after SAH, we conducted experiments in vitro. In line with the in vivo results, the in vitro data confirmed that necrosome formation was increased in the SAH condition (neurons exposed to Condition Medium). In addition, GSK872 reduced the phosphorylation of RIP3 and MLKL compared with the Condition Medium group. From the above experiments, we can conclude that RIP3 contributed to early brain injury by inducing necroptosis after SAH.

After SAH, a large number of neurons are heavily damaged by various pathological factors, resulting in apoptosis and necrosis. Accordingly, in the study of neuronal death after SAH, a vast majority of studies focused on apoptosis. In this study, we investigated necroptosis, a well-managed and elaborate cell death mechanism prompted by TNF-α activating RIP1 (O'Donnell et al., 2007). Activation of RIP1 recruited RIP3, and the interaction of these two proteins led to the phosphorylation of RIP3. The phosphorylation of RIP3 triggered its kinase activity, leading to more RIP3 autophosphorylation and MLKL phosphorylation. The combined interactions of RIP1-RIP3 and RIP3-MLKL together formed the necrosome that executed necroptosis (Sun et al., 2012; Wu et al., 2013). The role of RIP3 in necroptosis is more specific and critical than that of RIP1 as it presents the link between the initiator molecule RIP1 and the effector molecule MLKL. In fact, the overexpression of RIP3 can induce necroptosis even in the absence of RIP1 (Qiu et al., 2018). Therefore, RIP3 may serve as the vital switch

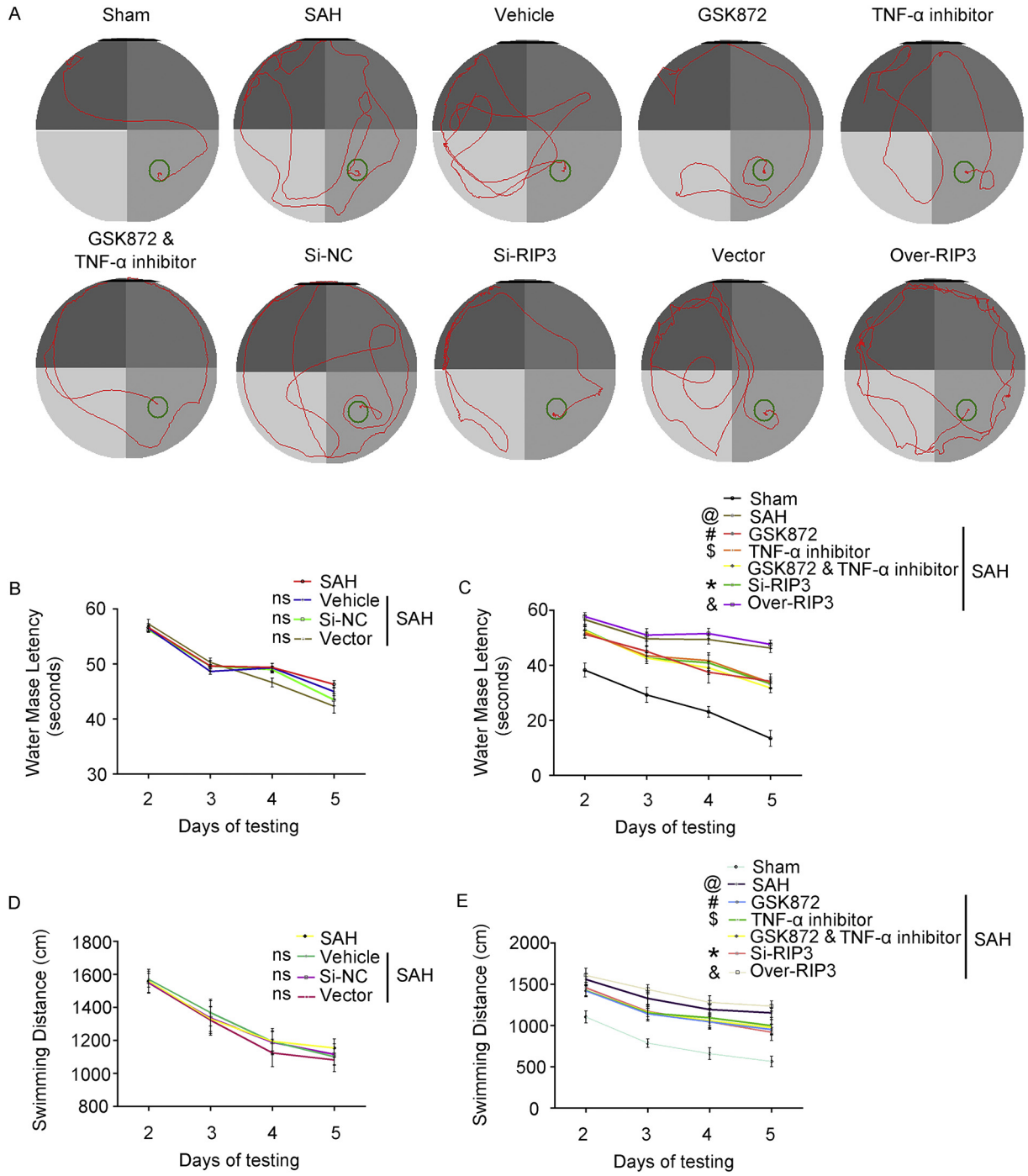

Fig. 7. Morris water maze (MWM) results. (A) Effect of GSK872, TNF-α inhibitor, Si-RIP3, and Over-RIP3 on total distance travelled in MWM test. Values were expressed as mean ± SEM. (B,·C) Motor learning was assessed by the change in the latency of escape. (D.E) Spatial learning was assessed by the swim distance that rat needed to find the visible (cued) versus the hidden (spatial) platforms in the water maze. Data were mean ± SEM; ns, no significant difference vs. SAH group; $^{@}P < 0.05$ vs. Sham group; $^{\#}P < 0.05$ vs. SAH + Vehicle group; $^{\$}P < 0.05$ vs. SAH + Vehicle group; $^{*}P < 0.05$ vs. SAH + Si-NC group; $^{\&}P < 0.05$ vs. SAH + Vector group; n = 6.

that fully activates necroptosis. RIP3 was also found to intervene in another cellular process, turning it pathological and deleterious to the cell by inducing necroptosis. Specifically, the process of cellular glucose metabolism has been shown to require the key enzyme pyruvate dehydrogenase complex (PDC) (Harris et al., 2002). Studies have reported that the abnormal activity of PDC was associated with cell senescence, and various diseases such as cancer, diabetes, and heart disease (Kaplon et al., 2013). Under the stimulation of TNF-α, RIP3 directly interacted with PDC and phosphorylated the threonine-135 site of its E3 subunit. Phosphorylation of this site led to a pathological increase in PDC activity, promoting cellular oxygen consumption and reactive oxygen species (ROS) production. ROS then oxidized a key cysteine on RIP1, which enhanced its kinase activity and promoted the formation of the necrosome and the execution of necroptosis (Yang et al., 2018)

Most of the diseases of the nervous system are related to neuronal damage. It has been thought that the death of neurons in these diseases was mainly carried out via necrosis and apoptosis. In recent years, necroptosis has also been found to be an important pathway of neuronal

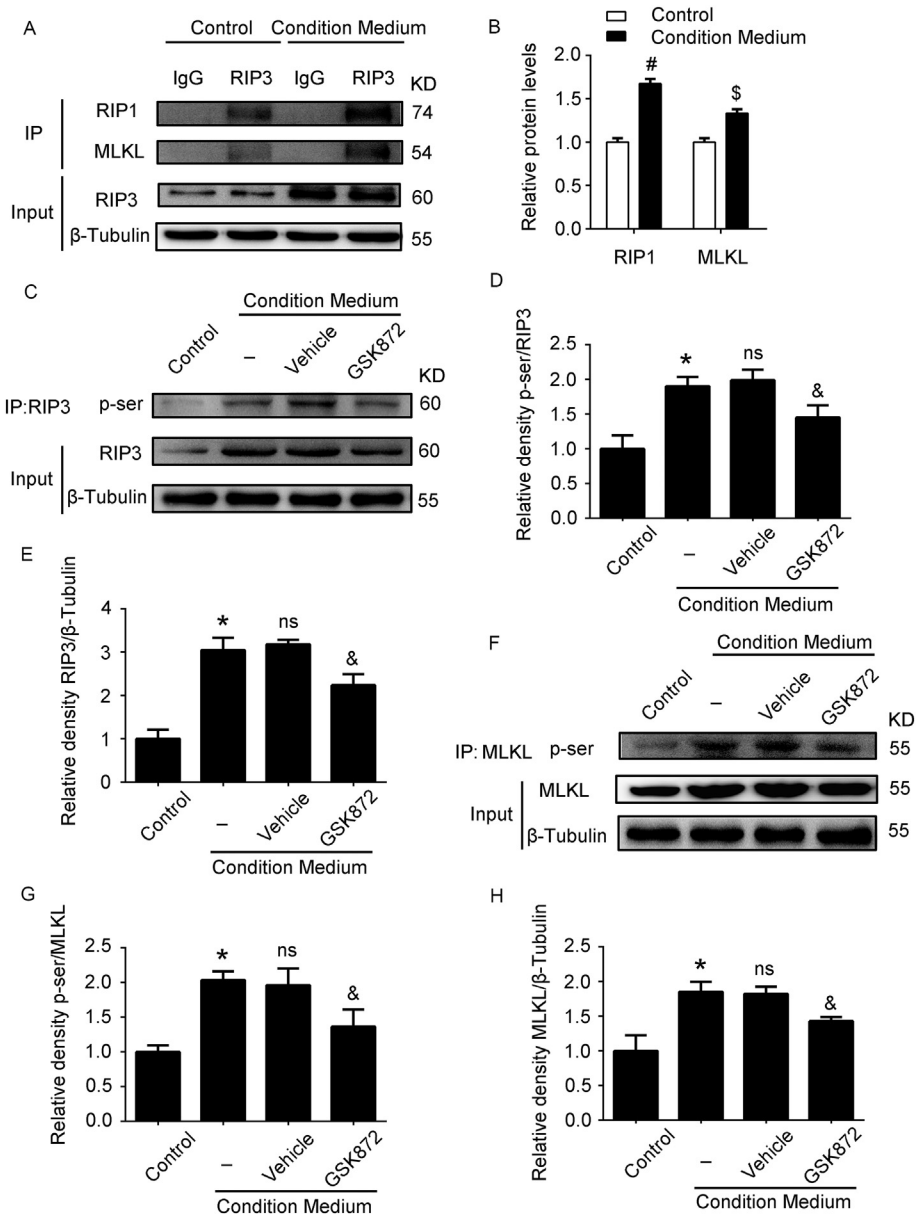

Fig. 8. The formation of necrosome in vitro. (A) Immunoprecipitation (IP) of cell lysates with RIP3 antibody. (B) Quantitative analysis of IP, $^{\#}P < 0.05$ and $^{\$}P < 0.05$ vs. Control group. (C) IP of cell lysates with RIP3 antibody. (D) Quantitative analysis of IP (p-ser/RIP3); $^{*}P < 0.05$ vs. Control group; ns, no significant difference vs. Condition Medium group; $^{\&}P < 0.05$ vs. Condition Medium + Vehicle group. (E) Quantitative analysis of IP (RIP3/β-tubulin); $^{*}P < 0.05$ vs. Control group; ns, no significant difference vs. Condition Medium group; $^{\&}P < 0.05$ vs. Condition Medium + Vehicle group. (F) IP of cell lysates with MLKL antibody. (G) Quantitative analysis of IP (p-ser/MLKL); $^{*}P < 0.05$ vs. Control group; ns, no significant difference vs. Condition Medium group; $^{\&}P < 0.05$ vs. Condition Medium + Vehicle group. (H) Quantitative analysis of IP (MLKL/β-tubulin); $^{*}P < 0.05$ vs. Control group; NS, no significant difference vs. Condition Medium group; $^{\&}P < 0.05$ vs. Condition Medium + Vehicle group. Data were mean ± SEM, n = 3.

death. Necroptosis has now been found to be the basis of many diseases including ischemic injury, neurodegenerative diseases, and viral infections. Numerous studies have also presented evidence that RIP3, as a key signaling molecule, is involved in the regulation of cellular immune responses and the necroptosis pathway. The death of mouse hippocampal neurons induced by TNF-α was mainly mediated by the CYLD-RIP1-RIP3-MLKL signaling pathway (Moquin et al., 2013). After intracerebroventricular injection of TNF-α in wild-type mice, a dose-dependent decrease in neuronal density was observed in the hippocampus. However, there was no significant decrease in the hippocampal neurons of RIP3-deficient mice, suggesting that RIP3 may play a role in the regulation of TNF-α-induced hippocampal neuronal damage (Liu et al., 2014). Necrostatin-1 (Nec-1), as a specific RIP1 inhibitor, effectively inhibited the RIP3 activation induced by RIP1 (Zhang et al., 2018). Nec-1 intervention in a middle cerebral artery occlusion (MCAO) model of stroke in mice significantly reduced infarct size and showed a dose-dependent improvement in neurological scores. Inhibiting the activation of RIP3 by blocking RIP1 prolonged neuroprotection and delayed necroptosis after the MCAO-induced ischemic brain injury. This means that necroptosis played an important role in ischemic brain injury and the inhibition of RIP1/RIP3-mediated necroptosis protected brain tissues from ischemic injury (Degterev et al., 2005). Studies of mouse ICH models have shown that Nec-1 reduced post-ICH hematoma volume, slowed cell death, reduced neurovascular injury, and improved neurological outcome in animals (King et al., 2014). Retinal damage is common in eye diseases and is often accompanied by neuronal damage. Normally, RIP3 is expressed at a low level in retinal cells, but when high intraocular pressure occurred, RIP3 levels rose rapidly. Therefore, it was speculated that necroptosis participated in the retinal cell death caused by high intraocular pressure (Nucci et al., 2005). In rat retinal ischemia-reperfusion models, necroptosis was shown to be mediated through an ERK1-RIP3 signaling pathway. The blockade of ERK caused the level of RIP3 to decrease considerably, and the survival rate of ganglion cells increased (Huang et al., 2013; Gao et al., 2014). In models of neonatal hypoxic-ischemic encephalopathy, the nervous system is stimulated with hypoxia-ischemia or lipopolysaccharide to produce neurotoxic substances such as IL-1β and MMP-9 in the brain. Both these models were able to activate the necroptosis signaling pathway (Savard et al., 2015). At present, there are still some areas for improvement in the basic research of the mechanisms of necroptosis.

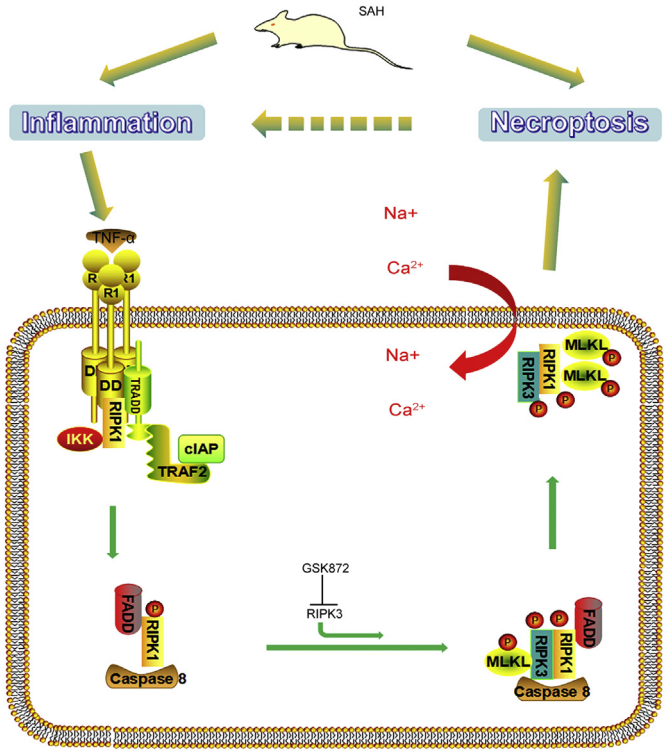

Fig. 9. The mechanism of necroptosis after SAH. After SAH occurs, increased TNF-α signaling through TNF receptor (TNFR) 1 induces the formation of complex I, which comprises RIP1, TNFR1-associated death domain protein (TRADD), TNF-receptor-associated factor 2 (TRAF2) and the cellular inhibitors of apoptosis (cIAP1 or cIAP2). RIP1 recruits and promotes RIP3 phosphorylation through the RIP homotypic interaction motif (RHIM). Then, a cytosolic complex IIb consisting of RIP1, RIP3, FADD, and caspase-8 forms. If caspase-8 is inhibited or RIP3 is expressed at high enough levels, the necrosome made up of RIPK1, RIPK3, and MLKL is formed. MLKL, which is phosphorylated by RIP3 at threonine 357 and serine 358 residues, is considered an executor of necroptosis. Phosphorylation promotes MLKL oligomerization and translocation to the plasma membrane, leading to membrane rupture and cell death.

Nevertheless, the vast body of published evidence clearly demonstrates that RIP3-mediated necroptosis is a critical cellular event that contributes to brain injury in a wide array of CNS diseases.

Although necroptosis is distinct from apoptosis, the close internal relationship between them permits the cell to switch from one to the other under different conditions (Han et al., 2009). The apoptotic pathway is usually a caspase-dependent process of cell death that requires the activation of caspase-induced signaling cascades (Redza-Dutordoir and Averill-Bates, 2016). In contrast, the signaling pathway of necroptosis has its own unique mechanisms, with the activation of the RIP1-RIP3 complex, the formation of the necrosome, and the phosphorylation of MLKL considered the most critical steps (Cho et al., 2009). Previous studies found that the inhibition of caspase-8 activity blocks the apoptotic signaling pathway and triggers the necroptosis pathway to take over. Specifically, the classical RIP1/RIP3 signaling pathway of necroptosis arrives at a point where the cell is faced with a choice. If caspase-8 is activated, the RIP1-RIP3 complex is cleaved and apoptosis occurs under the control of activated caspase-8. Conversely, if the activity of caspase-8 is inhibited, the complex formed by the phosphorylated RIP1 and RIP3 would predominate, and the death signal is transmitted downstream by RIP1-RIP3 (Ea et al., 2006). Therefore, regulation of the relative activity of the caspase-8 and RIP1-RIP3 complexes allows cells to switch between apoptosis and necroptosis. RIP3 functions at the crossroads of apoptosis and necroptosis and has an important regulatory role in the cell's choice of cell death pathway. In this study, we used GSK872 (1 μM) to inhibit RIP3 in vitro; according to a previous study, 1 μM GSK872 did not induce cytotoxicity or apoptosis in vitro, but higher concentrations (10 μM) did. (Mandal et al., 2014). For in vivo experiments, GSK872 treatment (3.3 mg/kg, intracerebroventricular injection) significantly inhibited phosphorylation of RIP3 and necroptosis in brain tissue of rats after SAH, however, we did not perform analysis to detect whether apoptotic cells were increased after GSK872 treatment. Meanwhile, as far as we know, there were no reports about whether inhibition of RIP3 by GSK872 treatment could switch necroptosis to apoptosis in brain tissue after SAH. Of course, this question would be explored in our future work.

SAH causes a series of neurophysiological changes in the body, and chain reactions of harmful pathological processes continue to occur even after the initial injury. The immune inflammatory responses after SAH may be caused by red blood cells or their lysates (Miller et al., 2014). Recent studies have shown that necroptosis can directly or indirectly cause inflammatory reactions, the main mechanisms including the release of a large amount of damage associated molecular patterns (DAMPs) and the activation of the NOD-like receptor protein 3 (NLRP3) inflammatory bodies (Lawlor et al., 2015). Inflammatory bodies contain receptor molecules and pro-caspase-1 macromolecules, and NLRP3-inflammatory-body activation is one of the important molecular mechanisms of the cell's inflammatory response. A previous study found that in a viral infection model, the RIP1-RIP3 complex promoted dynamin-related protein 1 (Drp1) transport to the mitochondria by activating guanosine triphosphatase, thereby activating NLRP3 inflammatory bodies. When the signaling pathways of DAMPs and NLRP3 were activated, the expression of TNF-α increased (Fiuza et al., 2003; Ferrari et al., 2006). TNF-α, which triggers a cascade of inflammatory reactions, is an important pro-inflammatory cytokine and a positive regulator of inflammation. Our current understanding of necroptosis is mostly derived from the study of the TNF signaling pathway. In this study, we found that the level of TNF-α in the CSF of rats was significantly increased following SAH induction. In addition, after treatment with TNF-α inhibitor, PI-positive cells were reduced in the SAH-injured brain, indicating that the SAH-induced necroptosis was at least partly induced by increasing TNF-α. Additionally, we found no change in the phosphorylation of RIP3 and MLKL or in measures of brain injury (BBB damage and edema) under the intervention of GSK872 compared with GSK872 + TNF-α. This could be because TNF-α inhibitor suppressed the necroptosis pathway upstream of RIP3, occluding any further effect of the RIP3 inhibitor GSK872. Under the effects of TNF-α inhibitor, the entire necroptosis pathway was suppressed. Collectively, we can speculate that the cell's inflammatory response gets activated after SAH, leading to an increase in TNF-α expression. Then, the classical RIP1/RIP3-mediated necroptosis is activated and kills neurons. Ultimately, extensive neuronal necroptosis further aggravates the inflammatory response.

Additionally, while our research was in progress, Fuxiang Chen et al. (2017b) and Keren Zhou et al. (2017) reported that Necrostatin-1 attenuates EBI after SAH in rats. Ting Chen et al. (2018) also reported that inhibiting RIP3 by GSK872 attenuates brain injury following SAH in rats induced by an endovascular perforation method. When these findings were taken together, we can conclude that both RIP1 and RIP3 participated in brain injury following SAH. This study has some technical limitations. Firstly, we only used adult, male rats to establish the SAH model in vivo but we often see older, female patients presenting with SAH stroke in the clinic. In vitro, we subjected microglia to OxyHb treatment to produce the Condition Medium, but blood contains many other relevant components such as iron ions, adenosine triphosphate, and plasmin. Secondly, our study only investigated the necroptosis pathway initiated by TNF-α signaling, while it is possible that endogenous cellular necroptosis may occur under a variety of stimuli. Therefore, there may be other mechanisms that influenced the results of this experiment. Finally, our use of a rat model to study brain damage mechanisms after SAH is a long way from a translational human study.

In summary, our study confirmed the RIP3-mediated necroptosis

occurred in the brain tissue of rats following SAH and played an essential role in SAH-induced brain injury. The in vitro model of SAH suggested that the release of TNF-α from activated microglia might be an important factor inducing necroptosis after SAH (Fig. 9). Our results further elucidated the mechanisms of cell death and its relationship with inflammation and brain injury after SAH. These findings may also present a potential therapeutic target for the amelioration of brain injury after SAH.

Supplementary data to this article can be found online at https://doi.org/10.1016/j.nbd.2019.05.004.

Declaration of competing interests

The authors declare no competing financial interests.

Acknowledgments

This work was supported by a grant from the National Natural Science Foundation of China (No. 81601007), National Key R&D Program of China (No. 2018YFC1312600 and 2018YFC1312601), Project of Jiangsu Provincial Medical Innovation Team (No. CXTDA2017003), Jiangsu Provincial Medical Youth Talent (No. QNRC2016728), Suzhou Key Medical Centre (No. Szzx201501), Scientific Department of Jiangsu Province (No. BE2017656), and Suzhou Government (LCZX201601).

References

Cahill, J., Calvert, J.W., Zhang, J.H., 2006. Mechanisms of early brain injury after subarachnoid hemorrhage. J. Cereb. Blood Flow Metab. 26 (11), 1341–1353.
Cai, Z., et al., 2014. Plasma membrane translocation of trimerized MLKL protein is required for TNF-induced necroptosis. Nat. Cell Biol. 16 (1), 55–65.
Cao, J., et al., 2018. Leucine-rich repeat kinase 2 aggravates secondary brain injury induced by intracerebral hemorrhage in rats by regulating the P38 MAPK/Drosha pathway. Neurobiol. Dis. 119, 53–64.
Chen, S., et al., 2013. P2X7R/cryopyrin inflammasome axis inhibition reduces neuroinflammation after SAH. Neurobiol. Dis. 58, 296–307.
Chen, X., et al., 2014. Translocation of mixed lineage kinase domain-like protein to plasma membrane leads to necrotic cell death. Cell Res. 24 (1), 105–121.
Chen, F., et al., 2017a. Necrostatin-1 attenuates early brain injury after subarachnoid hemorrhage in rats by inhibiting necroptosis. Neuropsychiatr. Dis. Treat. 13, 1771–1782.
Chen, F., et al., 2017b. Necrostatin-1 attenuates early brain injury after subarachnoid hemorrhage in rats by inhibiting necroptosis. Neuropsychiatr. Dis. Treat. 13, 1771–1782.
Chen, T., et al., 2018. Inhibiting of RIPK3 attenuates early brain injury following subarachnoid hemorrhage: possibly through alleviating necroptosis. Biomed. Pharmacother. 107, 563–570.
Cho, Y.S., et al., 2009. Phosphorylation-driven assembly of the RIP1-RIP3 complex regulates programmed necrosis and virus-induced inflammation. Cell 137 (6), 1112–1123.
Degterev, A., et al., 2005. Chemical inhibitor of nonapoptotic cell death with therapeutic potential for ischemic brain injury. Nat. Chem. Biol. 1 (2), 112–119.
Dondelinger, Y., et al., 2013. RIPK3 contributes to TNFR1-mediated RIPK1 kinase-dependent apoptosis in conditions of cIAP1/2 depletion or TAK1 kinase inhibition. Cell Death Differ. 20 (10), 1381–1392.
Dou, Y., et al., 2017. Tumor necrosis factor receptor-associated factor 6 participates in early brain injury after subarachnoid hemorrhage in rats through inhibiting autophagy and promoting oxidative stress. J. Neurochem. 142 (3), 478–492.
Ea, C.K., Deng, L., Xia, Z.P., Pineda, G., Chen, Z.J., 2006. Activation of IKK by TNFalpha requires site-specific ubiquitination of RIP1 and polyubiquitin binding by NEMO. Mol. Cell 22 (2), 245–257.
Etminan, N., 2015. Aneurysmal subarachnoid hemorrhage–status quo and perspective. Transl. Stroke Res. 6 (3), 167–170.
Feoktistova, M., et al., 2011. cIAPs block Ripoptosome formation, a RIP1/caspase-8 containing intracellular cell death complex differentially regulated by cFLIP isoforms. Mol. Cell 43 (3), 449–463.
Ferrari, D., et al., 2006. The P2X7 receptor: a key player in IL-1 processing and release. J. Immunol. 176 (7), 3877–3883.
Fiuza, C., et al., 2003. Inflammation-promoting activity of HMGB1 on human microvascular endothelial cells. Blood 101 (7), 2652–2660.
Gao, S., Andreeva, K., Cooper, N.G., 2014. Ischemia-reperfusion injury of the retina is linked to necroptosis via the ERK1/2-RIP3 pathway. Mol. Vis. 20, 1374–1387.
Han, W., Xie, J., Li, L., Liu, Z., Hu, X., 2009. Necrostatin-1 reverts shikonin-induced necroptosis to apoptosis. Apoptosis 14 (5), 674–686.
Harris, R.A., Bowker-Kinley, M.M., Huang, B., Wu, P., 2002. Regulation of the activity of the pyruvate dehydrogenase complex. Adv. Enzym. Regul. 42, 249–259.
He, M.M., et al., 2005. Small-molecule inhibition of TNF-alpha. Science 310 (5750), 1022–1025.
Holler, N., et al., 2000. Fas triggers an alternative, caspase-8-independent cell death pathway using the kinase RIP as effector molecule. Nat. Immunol. 1 (6), 489–495.
Huang, J.F., et al., 2013. Differential neuronal expression of receptor interacting protein 3 in rat retina: involvement in ischemic stress response. BMC Neurosci. 14, 16.
Kaplon, J., et al., 2013. A key role for mitochondrial gatekeeper pyruvate dehydrogenase in oncogene-induced senescence. Nature 498 (7452), 109–112.
Kawahara, A., Ohsawa, Y., Matsumura, H., Uchiyama, Y., Nagata, S., 1998. Caspase-independent cell killing by Fas-associated protein with death domain. J. Cell Biol. 143 (5), 1353–1360.
King, M.D., Whitaker-Lea, W.A., Campbell, J.M., Alleyne Jr., C.H., Dhandapani, K.M., 2014. Necrostatin-1 reduces neurovascular injury after intracerebral hemorrhage. Int. J. Cell Biol. 2014, 495817.
Laster, S.M., Wood, J.G., Gooding, L.R., 1988. Tumor necrosis factor can induce both apoptic and necrotic forms of cell lysis. J. Immunol. 141 (8), 2629–2634.
Lawlor, K.E., et al., 2015. RIPK3 promotes cell death and NLRP3 inflammasome activation in the absence of MLKL. Nat. Commun. 6, 6282.
Leclerc, J.L., et al., 2018. A comparison of pathophysiology in humans and rodent models of subarachnoid hemorrhage. Front. Mol. Neurosci. 11, 71.
Li, H., et al., 2014. Evaluation of the protective potential of brain microvascular endothelial cell autophagy on blood-brain barrier integrity during experimental cerebral ischemia-reperfusion injury. Transl. Stroke Res. 5 (5), 618–626.
Li, J., et al., 2016. Minocycline protects against NLRP3 inflammasome-induced inflammation and P53-associated apoptosis in early brain injury after subarachnoid hemorrhage. Mol. Neurobiol. 53 (4), 2668–2678.
Liu, S., et al., 2014. Necroptosis mediates TNF-induced toxicity of hippocampal neurons. Biomed. Res. Int. 2014, 290182.
Lucke-Wold, B.P., et al., 2016. Aneurysmal subarachnoid hemorrhage and Neuroinflammation: a comprehensive review. Int. J. Mol. Sci. 17 (4), 497.
Mandal, P., et al., 2014. RIP3 induces apoptosis independent of pronecrotic kinase activity. Mol. Cell 56 (4), 481–495.
Meylan, E., Tschopp, J., 2005. The RIP kinases: crucial integrators of cellular stress. Trends Biochem. Sci. 30 (3), 151–159.
Miller, B.A., Turan, N., Chau, M., Pradilla, G., 2014. Inflammation, vasospasm, and brain injury after subarachnoid hemorrhage. Biomed. Res. Int. 2014, 384342.
Moquin, D.M., McQuade, T., Chan, F.K., 2013. CYLD deubiquitinates RIP1 in the TNFalpha-induced necrosome to facilitate kinase activation and programmed necrosis. PLoS One 8 (10), e76841.
Moriwaki, K., Chan, F.K., 2013. RIP3: a molecular switch for necrosis and inflammation. Genes Dev. 27 (15), 1640–1649.
Murakami, K., et al., 2011. Subarachnoid hemorrhage induces gliosis and increased expression of the pro-inflammatory cytokine high mobility group box 1 protein. Transl. Stroke Res. 2 (1), 72–79.
Neulen, A., et al., 2018. Large vessel vasospasm is not associated with cerebral cortical hypoperfusion in a murine model of subarachnoid hemorrhage. Transl. Stroke Res.
Nucci, C., et al., 2005. Neurochemical evidence to implicate elevated glutamate in the mechanisms of high intraocular pressure (IOP)-induced retinal ganglion cell death in rat. Neurotoxicology 26 (5), 935–941.
O'Donnell, M.A., Legarda-Addison, D., Skountzos, P., Yeh, W.C., Ting, A.T., 2007. Ubiquitination of RIP1 regulates an NF-kappaB-independent cell-death switch in TNF signaling. Curr. Biol. 17 (5), 418–424.
Ofengeim, D., et al., 2015. Activation of necroptosis in multiple sclerosis. Cell Rep. 10 (11), 1836–1849.
Orozco, S., et al., 2014. RIPK1 both positively and negatively regulates RIPK3 oligomerization and necroptosis. Cell Death Differ. 21 (10), 1511–1521.
Qiu, X., Zhang, Y., Han, J., 2018. RIP3 is an upregulator of aerobic metabolism and the enhanced respiration by necrosomal RIP3 feeds back on necrosome to promote necroptosis. Cell Death Differ. 25 (5), 821–824.
Redza-Dutordoir, M., Averill-Bates, D.A., 2016. Activation of apoptosis signalling pathways by reactive oxygen species. Biochim. Biophys. Acta 1863 (12), 2977–2992.
Savard, A., et al., 2015. Neuronal self-injury mediated by IL-1beta and MMP-9 in a cerebral palsy model of severe neonatal encephalopathy induced by immune activation plus hypoxia-ischemia. J. Neuroinflammation 12, 111.
Schievink, W.I., Riedinger, M., Jhutty, T.K., Simon, P., 2004. Racial disparities in subarachnoid hemorrhage mortality: Los Angeles County, California, 1985-1998. Neuroepidemiology 23 (6), 299–305.
Shen, H., et al., 2017. Role for RIP1 in mediating necroptosis in experimental intracerebral hemorrhage model both in vivo and in vitro. Cell Death Dis. 8 (3), e2641.
Shi, L., et al., 2017. PCMT1 ameliorates neuronal apoptosis by inhibiting the activation of MST1 after subarachnoid hemorrhage in rats. Transl. Stroke Res. 8 (5), 474–483.
Shlomovitz, I., Zargrian, S., Gerlic, M., 2017. Mechanisms of RIPK3-induced inflammation. Immunol. Cell Biol. 95 (2), 166–172.
Sun, L., Wang, X., 2014. A new kind of cell suicide: mechanisms and functions of programmed necrosis. Trends Biochem. Sci. 39 (12), 587–593.
Sun, X., Lee, J., Navas, T., Baldwin, D.T., Stewart, T.A., Dixit, V.M., 1999. RIP3, a novel apoptosis-inducing kinase. J. Biol. Chem. 274 (24), 16871–16875.
Sun, X., Yin, J., Starovasnik, M.A., Fairbrother, W.J., Dixit, V.M., 2002. Identification of a novel homotypic interaction motif required for the phosphorylation of receptor-interacting protein (RIP) by RIP3. J. Biol. Chem. 277 (11), 9505–9511.
Sun, L., et al., 2012. Mixed lineage kinase domain-like protein mediates necrosis signaling downstream of RIP3 kinase. Cell 148 (1–2), 213–227.
Suzuki, H., Hasegawa, Y., Kanamaru, K., Zhang, J.H., 2010. Mechanisms of osteopontin-induced stabilization of blood-brain barrier disruption after subarachnoid hemorrhage in rats. Stroke 41 (8), 1783–1790.
Tao, L., et al., 2016. Therapeutic hypothermia attenuates tissue damage and cytokine

expression after traumatic brain injury by inhibiting necroptosis in the rat. Sci. Rep. 6, 24547.
Vandenabeele, P., Galluzzi, L., Vanden Berghe, T., Kroemer, G., 2010. Molecular mechanisms of necroptosis: an ordered cellular explosion. Nat. Rev. Mol. Cell Biol. 11 (10), 700–714.
Vercammen, D., et al., 1998. Inhibition of caspases increases the sensitivity of L929 cells to necrosis mediated by tumor necrosis factor. J. Exp. Med. 187 (9), 1477–1485.
Wang, L., Du, F., Wang, X., 2008. TNF-alpha induces two distinct caspase-8 activation pathways. Cell 133 (4), 693–703.
Wang, Y.Q., et al., 2012. Necrostatin-1 suppresses autophagy and apoptosis in mice traumatic brain injury model. Neurochem. Res. 37 (9), 1849–1858.
Wang, Z., Wu, L., You, W., Ji, C., Chen, G., 2013. Melatonin alleviates secondary brain damage and neurobehavioral dysfunction after experimental subarachnoid hemorrhage: possible involvement of TLR4-mediated inflammatory pathway. J. Pineal Res. 55 (4), 399–408.
Wang, Y., et al., 2014. Necroptosis inhibitor necrostatin-1 promotes cell protection and physiological function in traumatic spinal cord injury. Neuroscience 266, 91–101.
Wu, J., et al., 2013. Mlkl knockout mice demonstrate the indispensable role of Mlkl in necroptosis. Cell Res. 23 (8), 994–1006.
Wu, F., et al., 2017a. Acid fibroblast growth factor preserves blood-brain barrier integrity by activating the PI3K-Akt-Rac1 pathway and inhibiting RhoA following traumatic brain injury. Am. J. Transl. Res. 9 (3), 910–925.
Wu, L.Y., et al., 2017b. Roles of pannexin-1 channels in inflammatory response through the TLRs/NF-kappa B signaling pathway following experimental subarachnoid hemorrhage in rats. Front. Mol. Neurosci. 10, 175.
Xie, Z., et al., 2018 March. Recombinant Netrin-1 binding UNC5B receptor attenuates neuroinflammation and brain injury via PPARgamma/NFkappaB signaling pathway after subarachnoid hemorrhage in rats. Brain Behav. Immun. 69, 190–202.
Yang, Z., et al., 2018. RIP3 targets pyruvate dehydrogenase complex to increase aerobic respiration in TNF-induced necroptosis. Nat. Cell Biol. 20 (2), 186–197.
Yin, C., Huang, G.F., Sun, X.C., Guo, Z., Zhang, J.H., 2017. DLK silencing attenuated neuron apoptosis through JIP3/MA2K7/JNK pathway in early brain injury after SAH in rats. Neurobiol. Dis. 103, 133–143.
Yoon, S., Bogdanov, K., Kovalenko, A., Wallach, D., 2016. Necroptosis is preceded by nuclear translocation of the signaling proteins that induce it. Cell Death Differ. 23 (2), 253–260.
Yu, P.W., et al., 1999. Identification of RIP3, a RIP-like kinase that activates apoptosis and NFkappaB. Curr. Biol. 9 (10), 539–542.
Zhang, D.W., et al., 2009. RIP3, an energy metabolism regulator that switches TNF-induced cell death from apoptosis to necrosis. Science 325 (5938), 332–336.
Zhang, J., Yang, Y., He, W., Sun, L., 2016. Necrosome core machinery: MLKL. Cell. Mol. Life Sci. 73 (11 − 12), 2153–2163.
Zhang, L., Feng, Q., Wang, T., 2018. Necrostatin-1 protects against paraquat-induced cardiac contractile dysfunction via RIP1-RIP3-MLKL-dependent necroptosis pathway. Cardiovasc. Toxicol. 18 (4), 346–355.
Zhou, K., et al., 2017. RIP1-RIP3-DRP1 pathway regulates NLRP3 inflammasome activation following subarachnoid hemorrhage. Exp. Neurol. 295, 116–124.